Multiphase CFD Modelling of Stirred Tanks

By

Harish Appa

Thesis presented in partial fulfillment
for the Degree of Master of Science

Department of Mechanical Engineering
University of Cape Town
2007

ACKNOWLEDGEMENTS

I would like to thank the following people for their help, without which this work would not have possible.

Assoc. Prof. David Deglon and **Dr. Chris Meyer** my supervisors for their constant support, insightful advice, assistance and for always believing in me.

Dr. Nirmal Weerasekara for technical support, his priceless advice and guidance

Alice Siwale and **Darnell Engelbrecht** for their respective work, on which this thesis, being a continuation of their work, is based on.

Dwain Dunn for his technical help even when he was not part of CERECAM.

Jean Paul Pelteret, **Vaneshen Naidoo**, **Amy Barty** and **Case Bakker** for being excellent lab partners and friends. I am also really grateful for their help and support.

Dr. Wojciech Wyczalkowski, director of R&D at Philadelphia Mixing Solutions Ltd for his technical help

Dr. Peter Spicka, senior consulting engineer, CCP Team at Fluent Inc. for his technical help.

My parents, for their love, trust and encouragement and to whom I dedicate this work.

Simla Appa Sukhoo, my sister for her constant moral support and advice.

Neelan Rama for the hilarious and well-appreciated conversations during the thesis crisis moments.

Jean-Paul Pelteret, **Daniel Payaneeandee**, **Maureen Tanner** and **Vanessa Sew Chung Hong** for proof reading the thesis and their critical advice.

Last but not least all my friends for their constant support.

ACKNOWLEDGEMENTS

I would like to thank the following people for their help, without which this work would not have possible.

Assoc. Prof. David Deglon and **Dr. Chris Meyer** my supervisors for their constant support, insightful advice, assistance and for always believing in me.

Dr. Nirmal Weerasekara for technical support, his priceless advice and guidance

Alice Siwale and **Darnell Engelbrecht** for their respective work, on which this thesis, being a continuation of their work, is based on.

Dwain Dunn for his technical help even when he was not part of CERECAM.

Jean Paul Pelteret, **Vaneshen Naidoo**, **Amy Barty** and **Case Bakker** for being excellent lab partners and friends. I am also really grateful for their help and support.

Dr. Wojciech Wyczalkowski, director of R&D at Philadelphia Mixing Solutions Ltd for his technical help

Dr. Peter Spicka, senior consulting engineer, CCP Team at Fluent Inc. for his technical help.

My parents, for their love, trust and encouragement and to whom I dedicate this work.

Simla Appa Sukhoo, my sister for her constant moral support and advice.

Neelan Rama for the hilarious and well-appreciated conversations during the thesis crisis moments.

Jean-Paul Pelteret, **Daniel Payaneeandee**, **Maureen Tanner** and **Vanessa Sew Chung Hong** for proof reading the thesis and their critical advice.

Last but not least all my friends for their constant support.

ABSTRACT

Stirred tanks agitated with Rushton turbines are commonly used in industry, for instance mixing processes and flotation systems. The need for more efficient systems in industries has led to the study of fluid flow within the tanks upon agitation; so that a better understanding of the phenomena can help in the optimisation of the tanks. In the recent years, efforts have been made towards the development of predictive methods using computational fluid dynamics (CFD). Among the various numerical works presented, emphasis was laid mainly on single phase systems. However, due to the various processes involving gas-liquid systems, the need for multiphase modelling of stirred tanks became increasingly important. This has led to more research studies involving multiphase flows. Most of the work reported showed good prediction of the velocity data and the power draw, reasonable turbulence parameters. But, the prediction of the gas hold-up was rarely well established.

Therefore, the aim of this thesis, based on the numerical work presented by Engelbrecht (2006), is to investigate the discrepancies reported and to develop a multiphase model of a stirred tank agitated by a Rushton turbine. The commercially available CFD code FLUENT® was used to model the agitated gas-liquid system. The results were validated with the numerical work of Engelbrecht (2006) and the experimental work presented by Deglon (1998).

Two main cases were investigated, with a steady state and a transient approach. The QUICK scheme was used for the discretisation of the volume fraction and momentum and the first order upwind scheme for the discretisation of the turbulent kinetic energy and dissipation rate. The standard $k-\varepsilon$ turbulence model was used to account for the turbulent flow regime. A steady state MRF model was used for the investigation of the discrepancy reported by Engelbrecht (2006). The author reported that no convergence was achieved with such models. Solving the problem would have resulted in a good modelling approach for the prediction of gas dispersion, since steady state models are not computationally intensive. Three different boundary conditions, namely, a pressure outlet, an outflow and a velocity inlet, were used to model the outlet of the tank. The Euler-Euler multiphase model was used to simulate the gas-liquid system for the steady state model.

The sliding mesh model was used to simulate the transient case. Two different multiphase models, the Euler-Euler and the mixture model, were used for comparative purposes. Then, based on the findings a modified drag model of Schiller and Naumann was implemented and validated. This was used to account for the increase in drag caused by frothers.

The results for the velocity values and turbulence parameters were well predicted. They showed good correlation to the numerical work presented by Engelbrecht (2006). The prediction of the mean velocity in the bulk tank and the turbulence parameters at the impeller tip did not follow the experimental trend. However, the differences were attributed to the experimental techniques used. The gas hold-up was poorly predicted for all cases and none of the steady state models satisfied the continuity convergence criterion.

The convergence criterion problem was resolved with the unsteady state models. The latter were based

on the Euler-Euler and the mixture model at an impeller speed of 940 rpm. The models were both in accordance with the numerical investigation of Engelbrecht (2006). The results for both models followed the same trend in terms of mean velocity, power draw, gas hold-up and turbulence parameters. The turbulence parameters were over-predicted in highly turbulent regions with the mixture model. Nonetheless, the mixture model being a less computationally intensive than the Euler-Euler model was found reasonable for the prediction of gas dispersion. Furthermore, both models were found to poorly predict the flow at the gas-liquid interface. The flow above the baffles rose to an unrealistic amount, resulting in an unwanted entrainment of gas in the system.

Further investigations at impeller speeds at 630 rpm and 1260 rpm showed that the phenomenon was exacerbated with increasing impeller speed. However, the discrepancy was less significant at 630 rpm. The fluid flow at the different speeds was also validated with the experimental data of Deglon (1998). All the cases showed good correlation, however some discrepancies were observed at higher impeller speed with the prediction in the impeller region. The turbulence parameters were again over-predicted in the turbulent regions, which corroborated with the findings at 940 rpm suggesting a possible shortcoming of the mixture model over Euler-Euler model. It was further concluded, that the models failed to simulate the gas-liquid interface accurately. However, a system with a low impeller speed can be used for an agitated gas-liquid system.

The modified drag model, which accounted for the effect of frothers, gave acceptable results. An increase in the gas hold-up was observed with the increase in drag coefficient. However, the increase in gas hold-up was not proportional to the increase in drag coefficient. The increase in gas in the system resulted in the expected decrease in mean and root mean square velocity. On the other hand, the increase in turbulent kinetic energy was not observed. Similarly, the power draw decreased instead of the expected increase observed experimentally. Nonetheless, it was concluded that the approach of modifying the Schiller and Naumann was acceptable.

DECLARATION

1. I hereby grant the University of Cape Town free licence to reproduce for the purpose of research either the whole or any portion of the contents in any manner whatsoever of this dissertation.

2. I know the meaning of plagarism and declare that all of the work in this document, save for that which is properly acknowledged, is my own.

Signature Signed by candidate Date 21/11/2007...

Harish Appa

CONTENTS

List of Figures

LIST OF TABLES

NOMENCLATURE

a	Impeller blade width (m)
$\vec{a}$	Acceleration $(m.s^{-2})$
b	Impeller hub diameter (m)
C	Off bottom impeller clearance (m)
C_D	Drag coefficient
d	Impeller disc diameter (m)
d_p	Diameter of bubble of phase p (m)
D	Impeller diameter (m)
E_1	Energy spectrum function $(m^2.s^{-1})$
$\vec{F}_q$	External body force (N)
$\vec{F}_{lift,q}$	Lift force (N)
$\vec{F}_{vm,q}$	Virtual mass force (N)
f	Drag function
$\vec{g}$	Gravitational acceleration $m.s^{-2}$
h	Impeller blade height (m)
k	Turbulent kinetic energy $(m^2.s^{-2})$
K_{pq}	Interphase momentum coefficient
n	Frequency (s^{-1})
N	Impeller speed (s^{-1})
p	Static pressure (Pa)
Re	Reynolds number
$\vec{R}_{pq}$	Interaction force between phase p and q (N)
T	Tank diameter (m)
u_i	Velocity components $(m.s^{-1})$
$\overline{u}_i$	Mean velocity components $(m.s^{-1})$
u_i'	Fluctuating velocity components $(m.s^{-1})$
$\nabla\vec{U}_q$	Phase-weighted velocity
v	Velocity $(m.s^{-1})$
V	Volume (m^3)
w	Baffle width (m)
z	Vertical distance from tank bottom (m)

Greek Letters

α	Volume fraction
ϵ	Rate of dissipation of turbulence energy (m^2s^{-3})
μ	Viscosity (Pa)
ϕ	Gas hold-up
v	Kinematic viscosity $(m^2.s^{-1})$

NOMENCLATURE

a	Impeller blade width (m)
$\vec{a}$	Acceleration $(m.s^{-2})$
b	Impeller hub diameter (m)
C	Off bottom impeller clearance (m)
C_D	Drag coefficient
d	Impeller disc diameter (m)
d_p	Diameter of bubble of phase p (m)
D	Impeller diameter (m)
E_1	Energy spectrum function $(m^2.s^{-1})$
$\vec{F_q}$	External body force (N)
$\vec{F}_{lift,q}$	Lift force (N)
$\vec{F}_{vm,q}$	Virtual mass force (N)
f	Drag function
$\vec{g}$	Gravitational acceleration $m.s^{-2}$
h	Impeller blade height (m)
k	Turbulent kinetic energy $(m^2.s^{-2})$
K_{pq}	Interphase momentum coefficient
n	Frequency (s^{-1})
N	Impeller speed (s^{-1})
p	Static pressure (Pa)
Re	Reynolds number
$\vec{R}_{pq}$	Interaction force between phase p and q (N)
T	Tank diameter (m)
u_i	Velocity components $(m.s^{-1})$
$\overline{u}_i$	Mean velocity components $(m.s^{-1})$
u_i'	Fluctuating velocity components $(m.s^{-1})$
$\nabla \vec{U}_q$	Phase-weighted velocity
v	Velocity $(m.s^{-1})$
V	Volume (m^3)
w	Baffle width (m)
z	Vertical distance from tank bottom (m)

Greek Letters

α	Volume fraction
ϵ	Rate of dissipation of turbulence energy $(m^2 s^{-3})$
μ	Viscosity (Pa)
ϕ	Gas hold-up
υ	Kinematic viscosity $(m^2.s^{-1})$

μ_t	Turbulent dynamic viscosity $\left(kg.m^{-1}.s^{-1}\right)$
μ_q	Shear of phase q (Pa)
λ_q	Bulk viscosity of phase q
ρ	Density $\left(kg.m^{-3}\right)$
σ_D	Prandtl dispersion coefficient
τ_p	Particulate relaxation time

Subscripts

dr	drift
$drag$	drag
$lift$	lift
m	mixture
k, l, q, r	phase
t	turbulent
vm	virtual mass

Abbreviations

CFD	Computational Fluid Dynamics
LDA	Laser Doppler Anemometry
LDV	Laser Doppler Velocimetry
MRF	Multiple Reference Frames
MIBC	Methyl Iso Butyl Carbinol
PIV	Particle Image Velocimetry
PDE	Partial Differential Equation
QUICK	Quadratic Upstream Interpolation for Convective Kinetics
RANS	Reynolds-averaged Navier-Stokes
RMS	Root Mean Square
SIMPLE	Semi-Implicit Method for Pressure-Linked Equations
SM	Sliding Mesh
UDF	User Defined Function

GLOSSARY

Bulk region:	The region in the stirred tank excluding the impeller region
Discretisation:	Process by which a closed-form mathematical expression such as a differential equation is approximated to a system of algebraic equation
Grid or Mesh:	Arrangement of discrete points throughout a flow field
Impeller region:	The region encapsulating the impeller and swept by the outflow of the impeller
Navier Stoke Equation:	Mathematical expression to solve the governing equations
Numerical diffusion:	False or fictitious numerical error that occurs in convection-diffusion formulations
Partial differential equation:	An equation that involves an unknown function of several independent variables and its partial derivatives with respect to those variables
Residual:	Amount by which a governing finite-difference relation at the centre of the gridat the n^{th} iteration are not satisfied
Solver:	Computer program that is used to solve the computational model
Structured grid:	A grid where the grid points are placed in a flow field in a very irregular fashion
Unstructured:	A grid where the grid points are arranged in a consistent geometrical regularity

1 INTRODUCTION

1.1 OVERVIEW

Stirred tanks are widely used in chemical, biochemical and mineral processing industries for the blending of miscible and immiscible liquids, gas-liquid/liquid-liquid mass transfer, suspensions of solids and chemical reactions. The vessels differ in shape, volume, number of impellers and impeller type, which vary from mixing processes to flotation systems.

Figure 1.1 depicts a typical stirred vessel with a flat bottom, four equidistant baffles agitated by a Rushton turbine, and a six-bladed impeller. The content of the tank is mixed by the flow generated by the rotation of the impellers. In gas-liquid systems these vessels are very efficient for gas dispersion due to the high level of agitation produced by the Rushton turbine (Deglon, 1998). On the other hand, the baffles provide additional mixing by preventing solid body rotation. The stirred tanks are also able to offer unmatched flexibility and control over transport processes occurring within the vessel (Ranade, 2002). These characteristics make the mechanically agitated tank a very effective device for mixing and contacting a gas with a liquid (Tatterson, 1991).

Figure 1.1: Typical stirred tank

Through the years, more efficient vessels were required as a result of their wide application in industries. This has led to more work in optimising the system. The need for new designs meant that an understanding of the fluid dynamics of the tank was required. This mainly involved the determination of the velocity of the flow field and turbulence, which is described by the turbulent kinetic energy, dissipation rate and root mean square (RMS) velocity.

This started with the investigation of the flow field, with photographic measurement of velocity of water (Cutter, 1966) in a stirred tank for the description of local rates of energy dissipation or to examine the trailing vortex pair in the impeller region (Riet and Smith, 1975). Similarly, studies were performed for gas-liquid mixtures where gas dispersion was examined (Riet and Smith, 1973). These experimental techniques were further improved with the application of Laser Doppler Anemometry (LDA) (Costes and Coudrec, 1988; Wu and Patterson, 1989; Wu et al., 1989; Dyster et al., 1993; Kresta and Wood, 1993).

Despite the progress made, there was still a lack of detailed data concerning the flow field (Shäfer et al., 1997). Thus, efforts have been made towards the development of predictive methods using Computational Fluid Dynamics (CFD). Single phase flows have been the first step in the modelling of the stirred tanks. Coupled with experimental techniques that can provide considerable information about 3-dimensional flow (Mavros, 2001), such as Laser Doppler Velocimetry (LDV) (Armenante et al., 1997) and Particle Image Velocimetry (PIV) (Deen et al., 2002; Ranade et al., 2001), single phase flows were investigated numerically. Comprehensive single phase numerical work has been presented, particularly with investigation of discretisation scheme, turbulence models, grid resolution or impeller rotation models in view of enhancing the prediction of the fluid flow and the associated phenomena in stirred tank (Ranade et al., 1989; Kresta and Wood, 1991; Luo et al., 1993; Fokema et al., 1994; G. Tabor, 1996; Ranade, 1997; Brucato et al., 1998; Wechsler et al., 1999; Jenne and Reuss, 1991; Aubin et al., 2004; Hartmann et al., 2004; Javed et al., 2006; Deglon and Meyer, 2006).

However, most of the industries use processes involving gas-liquids systems. Among the many sub-processes involved in such systems, gas dispersion, described by the interfacial area, gas hold-up and bubble size distribution, has been an active research area due to its strong influence on gas-liquid mass transfer (Sun et al., 2006). Nevertheless, the multiphase modelling of stirred tanks has not been comprehensively investigated. Only a few research studies have been carried out where the hydrodynamics and gas dispersion have been numerically predicted (Bakker, 1992; Gosman et al., 1992; Bakker and Akker, 1994; Ranade and Akker, 1994; Morud and Hjertager, 1996; Ranade and Deshpande, 1999; Lane et al., 2002; Deen et al., 2002; Khopkar et al., 2005; Kerdouss et al., 2006). The development and understanding of the multiphase models can be used as the stepping stone for the modelling of the complex phenomena occurring within stirred tanks.

Among the various studies presented with regards to a gas-liquid system in a Rushton turbine agitated stirred tank, many of them had reported a poor prediction of the gas hold-up. Recently Engelbrecht (2006) presented a multiphase model based on the single phase work of Siwale (2004). The work presented by Engelbrecht (2006) was based on the Euler-Euler multiphase model. Both the MRF and the sliding mesh model were used. A grid dependence study was performed using the steady state MRF model, where no significant difference was observed. The author also reported a poor prediction of the gas hold-up and the inability to achieve convergence with the MRF model. The sliding mesh model with the MRF model used as an initial condition was recommended by the author.

1.2 SCOPE OF THESIS

Thus, the purpose of this thesis was to develop a gas-liquid multiphase numerical model based on the work presented by Engelbrecht (2006), such that acceptable and reliable information in terms of the flow field and the gas hold-up can be obtained. The steady state MRF model, being computationally less intensive than the transient sliding mesh model, is a convenient way to achieve the mentioned objectives. The discrepancies with regards to convergence with the steady state models were thus investigated. The appropriateness of a mixture multiphase model was investigated and the implementation of the effect of frothers was also looked at. Various models with different boundary conditions for the outlet, impeller rotation models (steady and unsteady) and multiphase models were used in view of understanding and developing an efficient way to predict the above-mentioned flow characteristics.

The thesis begins with a literature review (Chapter 2) which contains a brief description of the numerical techniques used for the development of both single phase models and multiphase models for stirred tanks, their applicability and appropriateness to the modelling of stirred tanks. This is concurrently supported with a review of the findings reported in previous studies. The next chapter covers the methodology or numerical approach (Chapter 3) used in modelling the multiphase models. The geometry of the numerical models were based on the experimental work presented by Deglon (1998). The associated boundary conditions, turbulence models, discretisation scheme, impeller rotation model and multiphase models were described where appropriate. This is followed by a description of the techniques used to determine the velocity, turbulence parameters and gas hold-up. The results and discussions are presented in Chapter 4, where the multiphase results were compared to the experimental work and numerical work presented by Deglon (1998) and Engelbrecht (2006). The conclusions drawn are presented in Chapter 5 and finally recommendations based on these are presented in Chapter 6.

2 LITERATURE REVIEW

The wide application of stirred tanks has led to many research studies including both experimental and numerical work. The experimental work first started with the visualisation of single phase fluid flow and was followed by the determination of hydrodynamics properties, such as velocity and turbulence parameters. This was used as a stepping stone for the investigation of multiphase flows where, in addition to the above-mentioned parameters, factors such as gas hold-up and residence time were looked at. Some limitations were however observed with the experimental techniques used and therefore the numerical investigation of single phase and thereafter multiphase flows became increasingly important. Various numerical works have been published to date, where the techniques used and the findings were presented. These are briefly explained in this chapter, which starts with a description of the computational approaches used, their appropriateness and followed by a review of the findings for multiphase flows. The computational and mathematical models described were all according to the FLUENT® user manual (Fluent Inc).

2.1 GOVERNING EQUATIONS

The governing equations of fluid flow represent mathematical statements of the conservation laws of physics (Versteeg and Malalasekera, 1995). The conservation equations are given by the equations for mass (continuity) and momentum (Navier-Stokes). These are time-averaged to yield Reynolds averaged Navier-Stokes equations. The energy equation is solved for flows involving heat transfer or compressibility.

2.1.1 CONTINUITY EQUATION

The equation for conservation of mass, or continuity, is given by:

$$\frac{\partial \rho}{\partial t} + \nabla \cdot (\rho \vec{v}) = S_m \tag{2.1}$$

where S_m is the mass added to the continuous phase from the dispersed second phase and any user-defined sources

2.1.2 NAVIER-STOKES EQUATION

The Navier-Stokes equations, which describe the conservation of momentum, are given by:

$$\frac{\partial (\rho \vec{v})}{\partial t} + \nabla \cdot (\rho \vec{v} \vec{v}) = -\nabla p + \nabla \cdot (\overline{\overline{\tau}}) + \rho \vec{g} + \vec{F} \tag{2.2}$$

where
- p is the static pressure
- $\overline{\overline{\tau}}$ is the stress tensor
- $\rho \vec{g}$ is the gravitational body force
- $\vec{F}$ is the external body forces

It relates the sum of the convective acceleration and local acceleration to the sum of the pressure gradient, the viscosity term and the external body forces.

The stress tensor is given by

$$\bar{\bar{\tau}} = \mu \left[\left(\nabla \vec{v} + \nabla \vec{v}^T \right) - \frac{2}{3} \nabla \cdot \vec{v} I \right] \tag{2.3}$$

where μ is the molecular viscosity
I is a unit tensor

2.1.3 TIME AVERAGING

This method decomposes the solution variables in the instantaneous (exact) Navier-Stokes equations into the mean (time-averaged) and fluctuating components.

Thus, the velocity components are given by:

$$u_i = \overline{u}_i + u_i' \tag{2.4}$$

where $\overline{u}_i$ and u_i' are the mean and fluctuating components (i = 1,2,3).

Similar equations are used for other scalar quantities such as pressure, energy, species concentration. The time averaged equations are substituted into the instantaneous continuity and momentum equations yields:

$$\frac{\partial \rho}{\partial t} + \frac{\partial}{\partial x_i} \left(\rho \overline{u}_i \right) = 0 \tag{2.5}$$

and

$$\frac{\partial \left(\rho \overline{u_i} \right)}{\partial t} + \frac{\partial \left(\rho \overline{u_i} \overline{u_j} \right)}{\partial x_j} = -\frac{\partial p}{\partial x_i} + \frac{\partial}{\partial x_j} \left[\mu \left(\frac{\partial \overline{u_i}}{\partial x_j} + \frac{\partial \overline{u_j}}{\partial x_i} - \frac{2}{3} \delta_{ij} \frac{\partial \overline{u_l}}{\partial x_l} \right) \right] + \frac{\partial}{\partial x_j} \left(-\rho \overline{u_i' u_j'} \right) \tag{2.6}$$

Equation 2.5 and 2.6 are known as the Reynolds-averaged Navier-Stokes (RANS) equations. Additional terms, $-\rho \overline{u_i' u_j'}$, known as the Reynolds stresses now appear in Equation 2.6. These must be modelled to close the RANS equation.

2.2 DISCRETISATION

Discretisation is the process by which a closed-form mathematical expression is approximated to a system of algebraic expression. The accuracy and the ability to physically model a system is partly dictated by the discretisation scheme and has three fundamental properties namely conservativeness, boundedness and transportiveness (Versteeg and Malalasekera, 1995). They also ensure the stability of the flow regime. Furthermore, the accuracy of the numerical solution depends on how close the discretised equations represent the PDE's (Ranade et al., 1989). Thus, higher order schemes, ensure that the schemes are less prone to numerical diffusion errors. The better the accuracy of the scheme or for a given accuracy, the smaller will be the grid required. However, higher schemes can be more computationally expensive, for cases where high grid resolution are necessary. Many studies, as described in Section 2.2.1, have been presented to date. They reported the effect of discretisation scheme on computational stirred tank models. Among those used, were upwind, central, QUICK, hybrid and the power-law discretisation scheme.

2.2.1 INVESTIGATION OF DISCRETISATION SCHEMES

Aubin et al. (2004) investigated three discretisation schemes, namely the upwind, higher upwind and the quadratic upwind differencing schemes. The authors found that the type of discretisation scheme

has little or no effect on the prediction of the mean velocities. However, the first order upwind method under-predicted the small swirling region below the impeller. The dimensionless kinetic energy was under-predicted for the three numerical schemes, but was more significant for the upwind scheme.

The power-law discretisation scheme was used for the research conducted by Javed et al. (2006). The velocities were accurately predicted, however the turbulent kinetic energy was under-predicted throughout the tank.

The work presented by Brucato et al. (1998) made a comparison between the standard hybrid-upwind and the QUICK discretisation scheme. The authors showed that the two schemes gave slightly different results with respect to the velocities, which were comparable to experimental values. The QUICK scheme predicted a slightly higher recirculation rate near the top and bottom of the tank.

Deglon and Meyer (2006) investigated the effect of the upwind central and QUICK discretisation scheme. The authors concluded, that for a case where the grid was not too coarse, the mean velocity was negligibly affected by the discretisation scheme used. In contrast, the turbulent kinetic energy was highly influenced by the discretisation scheme. The authors, concluded that a high order discretisation scheme was required for more accurate CFD predictions.

2.3 TURBULENCE MODELLING

Turbulence modeling of flow in stirred tanks has been of great interest to many researchers in view of obtaining a more detailed insight into the complex hydrodynamics and mixing process in a cost effective way. Several models are available; these can be categorized into two main groups, namely the Reynolds-Averaged Navier-Stokes (RANS) based modelling approach and the Large Eddy Simulation approach. The latter renders the Navier-Stokes equations tractable so that the small-scale turbulent fluctuations do not have to be directly simulated. They both introduce additional terms in the governing equations that need to be modelled in order to achieve a "closure" for the unknown variables. The RANS models are based on time averaged Reynolds equations, which greatly reduces the required computational effort. In contrast to the RANS model, in the LES the large eddies are explicitly computed in a time-dependent simulation using the "filtered" Navier-Stokes equations. The filtering process filters out the eddies whose scales are smaller than the filter width or grid spacing used.

2.3.1 THE STANDARD $k-\epsilon$ MODEL

The standard $k-\varepsilon$ is a two-equation model for which two transport equations, the turbulent kinetic energy, k, and its dissipation rate, ε, need to be solved in order to compute the Reynolds stresses. It is a semi-empirical model, based mainly on flows with high Reynolds numbers. Its robustness and its ability to give reasonable predictions of flow fields makes it a convenient model in various applications. However, the model is valid mainly for fully turbulent flows since in its derivation the flow is assumed fully turbulent and the effects of molecular viscosity are negligible (Marden and Bakker, 2003). The dispersed $k-\epsilon$ model used for the Euler-Euler multiphase model is described in Section 2.6.2. The flow near the solid surfaces was accounted by the standard wall function as proposed by Launder and Spalding (1974).

2.3.2 INVESTIGATION OF TURBULENCE MODELS

The choice of an appropriate turbulence model has been the subject of many research studies in the modeling of stirred tanks. The researchers have used different models which varied in complexity in view of obtaining experimentally comparable results. Among the turbulence models used, were the RNG $k-\varepsilon$, LES, $k-\omega$ and the $k-\varepsilon$ model. The observations and suggestions made by the various authors are described below.

Aubin et al. (2004) investigation's compared two different models, namely the RNG and the standard $k-\varepsilon$ models. The authors reported that there were no major differences between the mean radial and axial velocities. Furthermore, both models were found to poorly predict the turbulent kinetic energy. Siwale (2004) compared the effect of the two models and the author found that the standard $k-\varepsilon$ model showed good agreement to experimental data. The RNG model was found to significantly under-estimate the turbulent kinetic energy levels in the impeller discharge regions.

Jaworski and Zakrzewka (2002) determined the effect of turbulence on the quality of the CFD prediction by using six turbulence models, namely the standard $k-\varepsilon$, the RNG $k-\varepsilon$, the realizable $k-\varepsilon$, the Chen-Kim $k-\varepsilon$, the optimised $k-\varepsilon$ and the Reynolds Stress Model. The axial mean velocity was well predicted with the standard $k-\varepsilon$ and the Chen-Kim $k-\varepsilon$ turbulence model. The tangential velocity showed good accuracy irrespective of the turbulence model. The turbulent kinetic was under-predicted for all cases, however, the results for the standard $k-\varepsilon$ model agreed better to the experimental results.

The LES turbulence model has also been applied to model the fluid flow within stirred tanks. The mean velocity values and turbulence intensities were well predicted (Derksen and Akker, 1999; Eggels, 1996). However, Hartmann et al. (2004) reported an over-prediction of the tangential velocity component and the turbulent kinetic energy values. Even though, the LES model led to reasonably good results, it has been limited to only a few research studies, due to the high grid requirements and the computational expense involved.

On the other hand, the standard $k-\varepsilon$ model has been the mostly used turbulence model. Used in various numerical investigations, the model predicted the flow field and the velocity reasonably well (Javed et al., 2006; Ranade et al., 1989; Kresta and Wood, 1991; Montante et al., 2001; Ranade et al., 2001). But, the turbulence parameters were under-predicted (Ranade and Deshpande, 1999; Javed et al., 2006; Montante et al., 2001; Ranade et al., 2001) especially in the region close the the impeller blade. Moreover, Abujelala and Lilley (1984) showed that the model had some shortcomings with regards to the confined swirling flows. Research conducted by Brucato et al. (1998) showed that no advantage is offered by the use of modified coefficients in the $k-\varepsilon$ turbulence model.

It has often been noted in literature that the standard $k-\varepsilon$ model showed some discrepancies in the modelling of the turbulent flow characteristics occurring within stirred tanks. However, Deglon and Meyer (2006) reported that the inability of the standard $k-\varepsilon$ model to accurately predict the turbulent parameters was due to numerical errors. Thus, the authors suggested a higher order discretisation scheme and finer grids as similarly reported by Wechsler et al. (1999) and Aubin et al. (2004). This approach was gave better prediction of the turbulence parameters.

2.4 GRID RESOLUTION

The grid resolution is very important in any computational model and it highly influences the accuracy of the results. In the modelling of stirred tank it has proved crucial, especially in the prediction of the flow fields with the corresponding fluid velocities and turbulence parameters. Various numerical investigations have been presented to date, to substantiate that the grid resolution does indeed affect some of the flow regime in stirred tanks. Table 2.1 shows the maximum grid resolution used for different investigations. The respective height of the tank, T, and the domain which refers to the section of the tank modelled are also tabulated.

Table 2.1: Computational grid used in various studies

Reference	T(m)	Domain	No. of Cells
Single phase systems			
Ranade et al. (1989)	0.3	90°	6 900
Kresta and Wood (1991)	0.456	45°	23 400
Luo et al. (1993)	0.294	180°	151 200
Fokema et al. (1994)	0.15	90°	17 200
Harvey et al. (1995)	0.145	90°	619 750
Tabor et al. (1996)	0.270	180°	120 000
Ranade (1997)	0.3	180°	61 152
Brucato et al. (1998)		180°	97 400
Ng et al. (1998)	0.1	180°	239 3468
Wechsler et al. (1999)	0.152	90°	1 003 520
Jenne and Reuss (1991)	0.444	90°	194 532
Sahu et al. (1999)	0.5	90°	21 000
Hartmann et al. (2004)	0.15	360°	228 096
Aubin et al. (2004)	0.19	360°	350 000
Javed et al. (2006)	0.296	180°	112 480
Deglon and Meyer (2006)	0.15	180°	1 900 000
Multiphase systems			
Gosman (1992)	1.83	45°	8 100
Ranade and Van Den Akker (1994)	0.3	180°	13 500
Ranade and Deshpande (1999)	0.3	180°	176 400
Lane et al. (2002)	1	60°	43 920
Deen et al. (2002)	0.222	180°	370 944
Khopkar et al. (2005)	0.2	180°	352 640
Engelbrecht (2006)	0.14	180°	1 340 928

It can been seen in Table 2.1 that a range of grid resolution has been used in previous studies. The early research studies performed were restricted by the number of cells that could be used due to the computational resources available. The work presented showed good quantitative and qualitative correlation to experimental data for the prediction of the velocities (Bakker, 1992; Harvey-III et al., 1995; G. Tabor, 1996). However, some discrepancies were noted in the determination of the turbulence parameters

(Bakker, 1992). Thus, with the availability of better computing power, the effect of grid resolution was investigated (Brucato et al., 1998; Wechsler et al., 1999; Ng et al., 1998; Siwale, 2004). Ng et al. (1998) demonstrated good prediction for the velocities. However, the turbulent kinetic energy, k, was under-predicted by about 50% in the region near the impeller blade. This discrepancy was attributed to the grid size, time step size, wall region treatment, the discretization scheme and the turbulence model. Siwale (2004) reported that the general flow field and the mean fluid velocity were not strongly affected by the grid resolution. In contrast, it greatly affected the prediction of the turbulent kinetic energy. Similarly, Wechsler et al. (1999) reported that the poor predictions of the turbulence kinetic energy are mainly due to the grid resolution rather than an inadequacy of the turbulence model as commonly noted in various studies (Hartmann et al., 2004; Aubin et al., 2004).

2.5 IMPELLER ROTATION MODELLING

The flow in a stirred tank with baffles is quite complex to model as the baffle-impeller interaction results in a periodic and time dependent flow. Literature on CFD stirred tank modelling shows the different solution approaches that were used to incorporate the motion of the impeller. The most common ones are the sliding mesh, the multiple reference frames, the snapshot and the impeller boundary condition models.

2.5.1 MULTIPLE REFERENCE FRAMES MODEL

The multi-reference frames model (MRF) is a steady-state approximation where the individual cell zones move at different rotational or translational speeds. As it is a reasonable model of time-averaged flow, the MRF model can be used for applications where the rotor-stator interaction is weak.

The MRF model has been used in various research studies (Lane et al., 2002; Aubin et al., 2004; Deglon and Meyer, 2006). The investigations showed that the model is convenient in the prediction of the flow field within the tank as well as the prediction of the velocities of the fluid flow.

2.5.2 SLIDING MESH MODEL

The sliding-mesh model is a time-dependent model where the grid surrounding the rotating component physically moves, by rotating in a stepwise manner. It gives a realistic model of the impeller, since the grid surrounding it moves such that time-accurate simulation of the impeller-baffle interaction is achieved. However, this technique is computationally expensive and computational requirements become excessive for multiphase flows (Lane et al., 2002).

Even though the sliding mesh is computationally intensive, it has been used in various studies to date. For example, Javed et al.(2006), NG et al.(1998), Hartmann et al.(2004), Aubin et al. (2004), Brucato et al. (1998) and Deglon and Meyer (2006). The predicted results were generally acceptable with regard to the general flow field and the velocities. The turbulent kinetic energy values near the impeller were either over-predicted or under-predicted (Javed et al., 2006; Brucato et al., 1998). They were either attributed to the grid resolution or in some case the turbulence model (Ng et al., 1998).

In order to implement the sliding mesh model, two or more grids need to be defined, such that the adjacent grids can slide relative to each other, by either rotating or translating. At each time step, the interface flux is determined from the two specific zones namely the interior zone and one or more periodic zones. The periodic zones are obtained from the intersection/overlapping of the interface zones. Figure 2.1 shows a 2-dimensional schematic representation of grid intersection.

The interface zones are composed of faces A-B and B-C, and faces D-E and E-F. They intersected to give faces a-d, d-b, b-e, e-c, c-f. The overlapping of the zones produced faces d-b, b-e and e-c, to form the interior zones while a-d and c-f, to form the periodic zone. For instance the interface flux for cell IV is calculated using faces d-b and b-e instead of face D-E.

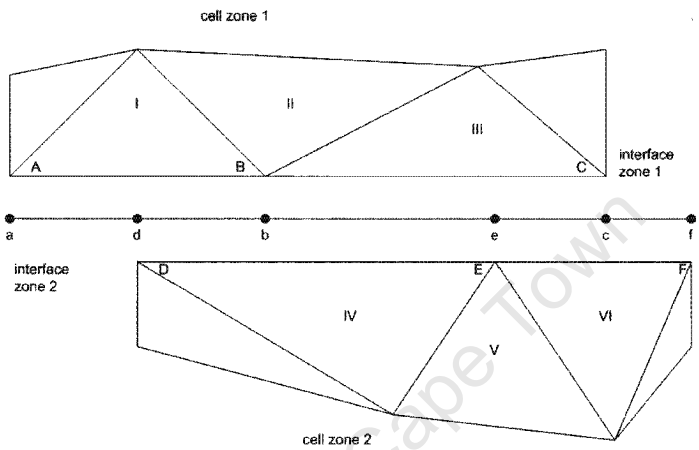

Figure 2.1: Schematic description of sliding mesh model (Fluent Inc)

When using time dependent techniques it is necessary to know when the solution has reached a steady state. Luo et al. (1993) reported that the flow pattern reaches steady state (cyclically repeatable) after about 6 impeller rotations for a 180° numerical model. A different approach was used by Tabor et al. (1996), where the MRF was used to generate the general flow field and thereafter the sliding mesh model was used to run for 10 impeller rotations. A similar technique was used by Wechsler (1999. This technique was used since as reported by the author, between 10 and 30 impeller rotations are required to overcome the start-up flow patterns. Deen et al. (2002) also used a similar approach where the sliding mesh model was run for 20 impeller rotations using the results of an earlier simulation. This method was also employed by Engelbrecht (2006) who used the MRF model initially and ran the sliding mesh model for 30 impeller rotations.

2.6 MULTIPHASE MODELS

The modelling of hydrodynamics and gas dispersion in stirred tanks is achieved through the use of multiphase models. The model divides the fluids in the vessel into a number of phases and treats them as separate sets of equations. These equations which include the transport equations for velocity, temperature and mass fractions with the inter-phase interactions through drag, heat and mass transfer are then solved. There are two ways to simulate multiphase flows, namely the Euler-Lagrange and the Euler-Euler approach.

In the Euler-Lagrangian approach, time-averaged Navier-Stokes equations are solved to describe a continuous fluid phase and a tracking method is used to describe the dispersed phase consisting of particles, bubbles or droplets. However, with this approach the model is only appropriate where the second phase occupies a low volume fraction. In contrast, the different phases are treated as inter-penetrating continua in the Euler-Euler approach.

2.6.1 EULER-EULER MODEL

The complex Euler-Euler model allows for the modelling of different separate, interacting phases. This is achieved, with the use of additional sets of conservation equations to the one used for single phase models. However, the modification requires the use of volume fraction for the description of the multiphase flow.

Volume Fractions

The volume fraction basically accounts for the space occupied by each phase, and the laws of conservation of mass and momentum are satisfied by each phase individually.

The volume occupied by a phase q, V_q, is given by:

$$V_q = \int_V \alpha_q dV \tag{2.7}$$

where α_q is the volume fraction of phase q

The sum of the volume fraction for all phases is always 1 in the control volumes:

$$\sum_{q=1}^{n} \alpha_q = 1 \tag{2.8}$$

The effective density of phase q is

$$\hat{\rho}_q = \alpha_q \rho_q \tag{2.9}$$

where ρ_q is the physical density of phase q.

Conservation of Mass and Momentum

Thus, for the conservation of mass the resulting continuity equation for phase q is given by:

$$\frac{\partial}{\partial t}(\alpha_q \rho_q) + \nabla \cdot (\alpha_q \rho_q \vec{v}_q) = \sum_{p=1}^{n} (\dot{m}_{pq} - \dot{m}_{qp}) + S_q \tag{2.10}$$

where
- $\vec{v}_q$ is the velocity of phase q
- $\dot{m}_{pq}$ is the mass transfer from the p^{th} to the q^{th} phase
- $\dot{m}_{qp}$ is the mass transfer from phase q to phase p
- S_q is the source term

On the other hand, the momentum balance for phase q is represented by:

$$\frac{\partial}{\partial t}\left(\alpha_q \rho_q \vec{v}_q\right) + \nabla \cdot \left(\alpha_q \rho_q \vec{v}_q \vec{v}_q\right) = -\alpha_q \nabla p + \nabla \cdot \bar{\bar{\tau}}_q + \alpha_q \rho_q \vec{g} +$$

$$\sum_{p=1}^{n}\left(\vec{R}_{pq} + \dot{m}_{pq}\vec{v}_{pq} - \dot{m}_{qp}\vec{v}_{qp}\right) + \left(\vec{F}_q + \vec{F}_{lift,q} + \vec{F}_{vm,q}\right) \tag{2.11}$$

where $\bar{\bar{\tau}}_q$ is the q^{th} phase stress-strain tensor:

$$\bar{\bar{\tau}}_q = \alpha_q \mu_q \left(\nabla \vec{v}_q + \nabla \vec{v}_q^T\right) + \alpha_q \left(\lambda_q - \frac{2}{3}\mu_q\right) \nabla \cdot \vec{v}_q \bar{\bar{I}} \tag{2.12}$$

where
- μ_q is the shear viscosity of phase q
- λ_q is the bulk viscosity of phase q
- $\vec{F}_q$ is the external body force
- $\vec{F}_{lift,q}$ is the lift force
- $\vec{F}_{vm,q}$ is the virtual mass force
- $\vec{R}_{pq}$ is the interaction force between phases
- p is the pressure shared by all phases
- $\vec{v}_{pq}$ is the interface velocity

The interaction term is given by:

$$\sum_{p=1}^{n} \vec{R}_{pq} = \sum_{p=1}^{n} K_{pq}\left(\vec{v}_p - \vec{v}_q\right) \tag{2.13}$$

where K_{pq} $(= K_{qp})$ is the interphase momentum exchange coefficient

Fluid-Fluid Momentum Exchange

The interphase momentum exchange, K_{pq}, coefficient is used to account for the momentum exchange between the phases, for instance between water and air bubbles and is given by:

$$K_{pq} = \frac{\alpha_q \alpha_p \rho_p f}{\tau_p} \tag{2.14}$$

where
- f is the drag function
- τ_p is the particulate relaxation time

The relaxation time is given by:

$$\tau_p = \frac{\rho_p d_p^2}{18\mu_q} \tag{2.15}$$

where d_p is the diameter of the bubbles of phase p.

The drag function depends on a drag coefficient C_D that is based on the relative Reynolds number(Re). There are three different drag models available in FLUENT®, namely the Schiller and Naumann model, the Morsi and Alexander model and the symmetric model. However, the Schiller and Naumann model as noted in literature (Kerdouss et al., 2006) was used.

The drag function for the Schiller and Naumann model takes the following form:

$$f = \frac{C_D Re}{24} \tag{2.16}$$

where

$$C_D = \begin{cases} 24\left(1 + 0.15Re^{0.687}\right)/Re & Re \leq 1000 \\ 0.44 & Re > 1000 \end{cases} \tag{2.17}$$

The relative Reynolds number for the primary phase q and the secondary phase p is given by :

$$Re = \frac{\rho_q |\vec{v}_p - \vec{v}_q| d_p}{\mu_q} \tag{2.18}$$

In contrast, the relative Reynolds number for the secondary phases p and r is given by:

$$Re = \frac{\rho_{rp} |\vec{v}_r - \vec{v}_p| d_{rp}}{\mu_{rp}} \tag{2.19}$$

where μ_{rp} is the mixture viscosity of phases p and r, and is equal to

$$\mu_{rp} = \alpha_p \mu_p + \alpha_r \mu_r \tag{2.20}$$

However, this correlation is suitable for particles moving in a stagnant liquid. Thus, to account for the effect of turbulence, a modified drag law is used (Bakker, 1992; Kerdouss et al., 2006). The relative Reynolds number is modified and is based on a modified viscosity term instead and is given by:

$$Re = \frac{\rho_q |\vec{v}_p - \vec{v}_q| d_p}{\mu^*} \tag{2.21}$$

where the modified viscosity term is the sum of the primary phase and a term proportional to the eddy viscosity. It is written as:

$$\mu^* = \mu_q + C\rho\frac{k^2}{\epsilon} \tag{2.22}$$

where C is a model parameter
ρ is the density
k is the turbulent kinetic energy per unit mass
ϵ is the turbulent energy dissipation

The parameter C is introduced to account for the decrease in slip velocity when a bubble is moving in a turbulent flow instead of in a still liquid (Bakker, 1992; Kerdouss et al., 2006).

But for the $k - \epsilon$ dispersed model the turbulent viscosity is related to k and ϵ through the semi-empirical expression:

$$\mu_t = \rho_q \frac{k_q^2}{\epsilon_q} \tag{2.23}$$

where q represents the primary phase

Thus,

$$\mu^* = \mu_q + C\mu_{t,q} \tag{2.24}$$

2.6.2 $k-\epsilon$ DISPERSED MODEL

The modelling of turbulence in multiphase simulation is relatively complex when compared to single-phase models. The $k-\epsilon$ dispersed model is one of the models available to account for turbulence in multiphase flows. It is appropriate where the concentrations of the secondary phases are low and inter-particle collisions are negligible.

The Reynolds stress tensor for the continuous phase is given by:

$$\overline{\overline{\tau}}_q'' = -\frac{2}{3}\left(\rho_q k_q + \rho_q \mu_{t,q} \nabla \cdot \vec{U}_q\right)\overline{\overline{I}} + \rho_q \mu_{t,q}\left(\nabla \vec{U}_q + \nabla \vec{U}_q^T\right) \tag{2.25}$$

where $\nabla \vec{U}_q$ is the phase-weighted velocity
$\mu_{t,q}$ is the turbulent fluid dynamic viscosity
k_q is the turbulent kinematic viscosity

The two transport equations, for k and ϵ that need to be solved for this model are as follows:

$$\frac{\partial}{\partial t}\left(\alpha_q \rho_q k_q\right) + \nabla \cdot \left(\alpha_q \rho_q \vec{U}_q k_q\right) = \nabla \cdot \left(\alpha_q \frac{\mu t, q}{\sigma_k} \nabla k_q\right) + \alpha_q G_{k,q} - \alpha_q \rho_q \epsilon_q + \alpha_q \rho_q \Pi_{k_q} \tag{2.26}$$

and

$$\frac{\partial}{\partial t}\left(\alpha_q \rho_q \epsilon_q\right) + \nabla \cdot \left(\alpha_q \rho_q \vec{U}_q \epsilon_q\right) = \nabla \cdot \left(\alpha_q \frac{\mu_{t,q}}{\sigma_\epsilon} \nabla \epsilon_q\right) + \alpha_q \frac{\epsilon_q}{k_q}\left(C_{1\epsilon} G_{k,q} - C_{2\epsilon} \rho_q \epsilon_q\right) + \alpha_q \rho_q \Pi_{\epsilon_q} \tag{2.27}$$

where G_{k_q} is the production of turbulent kinetic energy

The turbulent viscosity is related to the turbulent kinetic energy and the dissipation rate of turbulent kinetic energy via

$$\mu_{t,q} = \rho_q C_\mu \frac{k_q^2}{\epsilon_q} \tag{2.28}$$

Π_{k_q} and $\Pi\epsilon_q$ represent the influence of the dispersed phase on the continuous phase and are as follows:

$$\Pi_{k_q} = \sum_{p=1}^{M} \frac{K_{pq}}{\alpha_q \rho_q}\left(k_{pq} - 2k_q + \vec{v}_{pq} \cdot \vec{v}_{dr}\right) \tag{2.29}$$

where $\vec{v}_{pq}$ is the relative velocity
$\vec{v}_{dr}$ is the drift velocity
k_{pq} is the covariance of the velocities of the continuous phase q and the dispersed phase l

and

$$\Pi_{\epsilon_q} = C_{3\epsilon} \frac{\epsilon}{k_q} \Pi_{k_q} \tag{2.30}$$

Table 2.2 outlines the various model constants used in the turbulence model.

Table 2.2: Values of coefficients for $k-\epsilon$ turbulence model as used in FLUENT®

$C_{1\varepsilon}$	$C_{2\varepsilon}$	$C_{3\varepsilon}$	C_{μ}	σ_k	σ_{ε}
1.44	1.92	1.2	0.09	1	1.3

All the other terms have the same meaning as in the single phase $k-\epsilon$ model and the various models constants used in the turbulence model are tabulated in Table 2.2.

2.6.3 MIXTURE MODEL

The mixture model uses a different approach the Euler-Euler model, where the system is modelled as a single-fluid. The phases can be inter-penetrating such that the volume fractions α_q and α_p for a control volume can be equal to any value between 0 and 1, depending on the fluid system used. The model also allows the phases to move at different slip velocities. The continuity, momentum, energy and the algebraic expressions for the relative velocities are based on a mixture determined on the space occupied by the different phases involved rather than a set of equations for each phase. Thus, the mixture model is computationally less intensive than the Euler-Euler model, where a set of equations for each phase has to be solved.

Conservation of Mass and Momentum

The continuity equation for the mixture model is given by:

$$\frac{\partial}{\partial t}\left(\rho_m\right)+\nabla\cdot\left(\rho_m\vec{v}_m\right)=0 \tag{2.31}$$

where $\vec{v}_m$, the mass averaged velocity is determined by:

$$\vec{v}_m=\frac{\sum_{k=1}^{m}\alpha_k\rho_k\vec{v}_k}{\rho_m} \tag{2.32}$$

and ρ_m the mixture density

$$\rho_m=\sum_{k=1}^{m}\alpha_k\rho_k \tag{2.33}$$

where α_k is the volume fraction of phase k

The momentum equation for the mixture is determined by summing the individual momentum equations for all phases and is given by:

$$\frac{\partial}{\partial t}\left(\rho_m\vec{v}_m\right)+\nabla\cdot\left(\rho_m\vec{v}_m\vec{v}_m\right)=-\nabla p+\nabla\cdot\left[\mu_m\left(\nabla\vec{v}_m+\nabla\vec{v}_m^T\right)\right]+\rho_m\vec{g}+\vec{F}+\nabla\cdot\left(\sum_{k=1}^{n}\alpha_k\rho_k\vec{v}_{dr,k}\vec{v}_{dr,k}\right) \tag{2.34}$$

where n is the number of phases
$\vec{F}$ is the body force

The viscosity the mixture μ_m is given by:

$$\mu_m=\sum_{k=1}^{n}\alpha_k\mu_k \tag{2.35}$$

$\vec{v}_{dr,k}$ is the drift velocity for the secondary phase k:

$$\vec{v}_{dr,k} = \vec{v}_k - \vec{v}_m \tag{2.36}$$

Relative Velocity and Drift Velocity

The relative velocity (also referred to as the slip velocity) is defined as the velocity of a secondary phase (p) relative to the velocity of the primary phase (q):

$$\vec{v}_{pq} = \vec{v}_p - \vec{v}_q \tag{2.37}$$

The mass fraction for any phase (k) is given by

$$c_k = \frac{\alpha_k \rho_k}{\rho_m} \tag{2.38}$$

The following expression is obtained from the drift velocity and the relative velocity ($\vec{pq}$):

$$\vec{v}_{dr,p} = \vec{v}_{pq} - \sum_{k=1}^{n} c_k \vec{v}_{qk} \tag{2.39}$$

An algebraic slip formulation is used for the mixture model. The basic assumption of the algebraic slip mixture model is that to prescribe an algebraic relation for the relative velocity, a local equilibrium between the phases should be reached over short spatial length scale. The form of the relative velocity if given by:

$$\vec{v}_{pq} = \frac{\tau_p}{f_{drag}} \frac{(\rho_p - \rho_m)}{\rho_p} \vec{a} \tag{2.40}$$

where τ_p is the relaxation time and f is the drag function which is given by Equation 2.15 and Equation 2.16 respectively.

The acceleration, $\vec{a}$, is given by:

$$\vec{a} = \vec{g} - (\vec{v}_m \cdot \nabla)\, \vec{v}_m - \frac{\partial \vec{v}_m}{\partial t} \tag{2.41}$$

For turbulent flows, the relative velocity contains a diffusion term due to the dispersion appearing in the momentum phase for the dispersed phase. Therefore, the relative velocity is of the form:

$$\vec{v}_{pq} = \frac{(\rho_p - \rho_m)\, d_p^2}{18 \mu_q f_{drag}} \vec{a} - \frac{\nu_m}{\alpha_p \sigma_D} \nabla \alpha_q \tag{2.42}$$

where ν_m is the mixture turbulent viscosity
σ_D is the Prandtl dispersion coefficient

2.7 REVIEW OF MULTIPHASE CFD STUDIES

The fluid flow in the multiphase system is not much different to the single phase system. In a gas-liquid system, the accumulation of gas bubbles trapped by the centrifugal force of the trailing vortices, is observed. The energy dissipation increases at the impeller tip but decreases at both the impeller stream and in the bulk region. The increase in the dissipation energy substantially increases the flow around the impeller region and therefore the performance of the system (Ranade and Deshpande, 1999). Various research work based on multiphase flows have been published to date and is presented below.

Gosman et al. (1992) investigated the turbulent flow of a solid-liquid and a gas-liquid system. The Eulerian model was employed and the effect of the turbulent flow regime was modelled with the $k-\varepsilon$ model. The prediction of the velocity profile for the gas-liquid flow showed moderate agreement to experimental data. The void fraction near the free surface and the upper vortex was under-predicted. Similar trends were observed in the impeller stream and in the lower vortex. The discrepancy between experimental and numerical predictions was attributed to the assumptions of a constant bubble size, a spherical bubble shape and the use of a coarse grid.

Ranade and Van Den Akker (1994) used the computational snapshot model coupled with the standard $k-\varepsilon$ model and the Eulerian multiphase model. The authors found a relatively good agreement for the axial and tangential velocities. The predicted turbulent kinetic energy correlated poorly with the experimental data in some regions of the tank. However, the qualitative prediction of the gas hold-up agreed reasonably well to experimental data, with the common gas distribution pattern.

Bakker and Van Den Akker (1994) simulated a gas-liquid model which used a single phase flow pattern as input for an in-house code. The latter was used to calculate the gas hold-up, bubble break-up, bubble coalescence, bubble size, local interfacial area and local mass transfer. The gas hold-up was generally well predicted. However, discrepancies were found in the outflow of the impeller and were attributed to the lack of good impeller models.

Morud and Hjertager (1996) used a two dimensional model of a stirred tank, using the Eulerian model with the standard $k-\varepsilon$ to simulate the multiphase and the turbulent flow regime respectively. The authors showed that the gas velocity correlated well with experimental results. The gas hold-up was adequately predicted and was within the error range of experimental data.

Ranade and Deshpande (1999) simulated a stirred tank using the standard $k-\varepsilon$ turbulence model and the computational snapshot model. The authors were able to capture the main features of gas-liquid flow in stirred tanks with this approach. They also reported that this method is adequate for simulating flow characteristics in the bulk region of the vessels.

Lane et al. (2002) simulated the gas-liquid flow with the Eulerian model and the turbulent flow regime using the standard $k-\varepsilon$ turbulence model. The authors reported good gas prediction pattern and the correct trends in local bubble size in the tank. Even though, the gas hold-up was qualitatively well predicted, it was quantitatively under-predicted. This was attributed to the specification of the bubble drag coefficient.

Deen et al. (2002) investigated the two-phase system using the Eulerian model and the standard $k-\varepsilon$ turbulence model. The numerical results were compared to experimental data, and there was good agreement for the radial gas velocity. However, the axial gas velocities in the impeller discharge stream was over-predicted. The flow characteristics below and above the impeller were well predicted. The authors also reported that the presence of gas causes a 30% decrease in the maximum velocity in the radial jet.

Gentric et al. (2005) published work was based on the Eulerian model and the standard $k-\varepsilon$ turbulence model. The authors compared the performance of two gas-liquid reactors, one being a scaled-up version of the other. It was found that the global structure for the two tanks were similar. The authors

also reported good quantitative agreement with experimental data for gas hold-up.

Khopkar et al. (2005), also used a similar approach as previous authors, with the Eulerian multiphase model and the standard $k-\varepsilon$ model. The computational snapshot approach was used for the modelling of the impeller rotation. The computational model correctly captured the overall flow field generated. However, the author reported an over-prediction of the radial and tangential velocities in the impeller discharge stream. The comparison of predicted values of the gas hold-up with the experimental data showed some discrepancies. This was attributed to the way the experimental data was processed.

Kerdouss et al. (2006) investigated the gas dispersion and the flow regime in a double turbine stirred tank. The author used the Eulerian multiphase model and the dispersed $k-\varepsilon$ model to account for the turbulent flow. The numerical prediction of the gas hold-up agreed well with the experimental data. Similar results were reported for the bubble size distributions.

Sun et al. (2006) used the standard $k-\varepsilon$ model and the Inner-Outer (I-O) model to simulate the impeller rotation. The author reported a good qualitative prediction for the gas hold-up. The gas hold-up near the surface agreed reasonably to experimental data well near the liquid surface but showed some deviations in the bulk region.

Engelbrecht (2006) recently investigated a numerical model of a stirred tank. The author used the Euler-Euler multiphase model and the dispersed $k-\varepsilon$ turbulence model. Both the MRF and the sliding mesh model were used to simulate the impeller rotation. The results for both, the MRF model and the sliding mesh model, showed good correlation for the prediction of the velocity values, turbulence data and power draw. However, the acceptable convergence criterion for continuity of 1×10^{-3} was not met for any of the steady state models. The effect of grid resolution on the solution domain was also investigated with the MRF model. The author reported no considerable differences between the sets of data, for mean velocity values, the turbulence parameters, the power draw and gas hold-up. The MRF model was also used as an initial condition for the sliding mesh model. The gas hold-up for all cases investigated was under-predicted. The author concluded that the MRF model should be used as an initial condition for the modelling of multiphase flows in stirred tanks.

2.8 DISCUSSION

According to the various numerical investigations presented, the predictions of the mean velocity and the power draw were reasonably good. However, some authors reported some discrepancies in the prediction of the turbulence parameters. This may be attributed to the low grid resolution used and the failure to capture the relevant turbulent flow. The Euler-Euler multiphase model and the $k-\varepsilon$ turbulence model were most widely used.

The main concern was the modelling of the gas phase where the prediction of the gas hold-up varied for the different studies presented. Reasonably good gas hold-up values were obtained by Bakker and Van Den Akker (1994), Morud and Hjertager(1996), Gentric et al. (2005), Kerdouss et al. (2006) and recently Sun et al. (2006). However, all the investigations differed in their approach. The good prediction

presented by Bakker and Van Den Akker (1994) was based on an in-house code named GHOST!. The authors also considered the effect of the turbulent flow field on a bubble. This was achieved by modifying the viscosity to result in a decrease in the slip velocity. The investigation performed by Morud and Hjertager(1996) was based on a two dimensional model of the stirred tank. The work presented by Gentric et al. (2005) for an industrial gas-liquid reactor was based on a gas-liquid-solid flow where the liquid-solid mixture was treated as a pseudo-liquid phase. Kerdouss et al. (2006) investigated a double turbine stirred tank and used a fully unstructured mesh. The authors also used the same approach as Bakker and Van Den Akker (1994) to account for the effect of turbulence on the drag correlation of Schiller and Naumann. The numerical work recently presented by Sun et al. (2006) was based on a surface aerated stirred tank.

Khopkar et al. (2005) and Lane et al. (2002) both reported poor prediction of the gas hold-up. Both models were based on the Euler-Euler multiphase model. However, the computational snapshot model was used by Khopkar et al. (2005) and the MRF model by Lane et al. (2002). Thus, it can be observed that the only acceptable models for prediction of gas dispersion were either based on an in-house code or based on systems other than the Rushton turbine stirred vessels.

Based on the studies in the literature, it is clear that the development of an acceptable model for the modelling of a gas-liquid system for a stirred tank is needed. The current study is a continuation of the multiphase work developed by Engelbrecht (2006), and is aimed at investigating the discrepancies observed by the author and to produce a reliable gas-liquid numerical model. Firstly, the steady and unsteady state models will be investigated. Then, based on the findings the effect of frothers as suggested by Engelbrecht (2006) will be studied.

presented by Bakker and Van Den Akker (1994) was based on an in-house code named GHOST!. The authors also considered the effect of the turbulent flow field on a bubble. This was achieved by modifying the viscosity to result in a decrease in the slip velocity. The investigation performed by Morud and Hjertager(1996) was based on a two dimensional model of the stirred tank. The work presented by Gentric et al. (2005) for an industrial gas-liquid reactor was based on a gas-liquid-solid flow where the liquid-solid mixture was treated as a pseudo-liquid phase. Kerdouss et al. (2006) investigated a double turbine stirred tank and used a fully unstructured mesh. The authors also used the same approach as Bakker and Van Den Akker (1994) to account for the effect of turbulence on the drag correlation of Schiller and Naumann. The numerical work recently presented by Sun et al. (2006) was based on a surface aerated stirred tank.

Khopkar et al. (2005) and Lane et al. (2002) both reported poor prediction of the gas hold-up. Both models were based on the Euler-Euler multiphase model. However, the computational snapshot model was used by Khopkar et al. (2005) and the MRF model by Lane et al. (2002). Thus, it can be observed that the only acceptable models for prediction of gas dispersion were either based on an in-house code or based on systems other than the Rushton turbine stirred vessels.

Based on the studies in the literature, it is clear that the development of an acceptable model for the modelling of a gas-liquid system for a stirred tank is needed. The current study is a continuation of the multiphase work developed by Engelbrecht (2006), and is aimed at investigating the discrepancies observed by the author and to produce a reliable gas-liquid numerical model. Firstly, the steady and unsteady state models will be investigated. Then, based on the findings the effect of frothers as suggested by Engelbrecht (2006) will be studied.

3 NUMERICAL APPROACH

The flow processes in stirred tanks are defined by mathematical models, which are non-linear, coupled partial differential equations. These are the flow equations for the conservation of mass, momentum and turbulence quantities which are solved numerically. The numerical process is performed by having discrete information at finite number of locations, or grid points, which replaces the exact solution of the partial differential equations. The PDE's are solved with the definition of boundary conditions, and controlled by the discretisation scheme and the grid resolution. This chapter encompasses the different techniques and approaches used in this investigation. This includes the description of the geometry, which was based on the experimental work presented by Deglon (1998). The computational model, the boundary conditions and the grid resolution are further described. The data measurement techniques employed for the determination velocity values, turbulent parameters and gas hold-up are then explained.

3.1 GEOMETRY

The stirred tank used was a standard configuration vessel, with a flat bottom, four equidistant baffles, agitated by a six-bladed Rushton turbine. The geometry used for this study is shown in Figure 3.1.

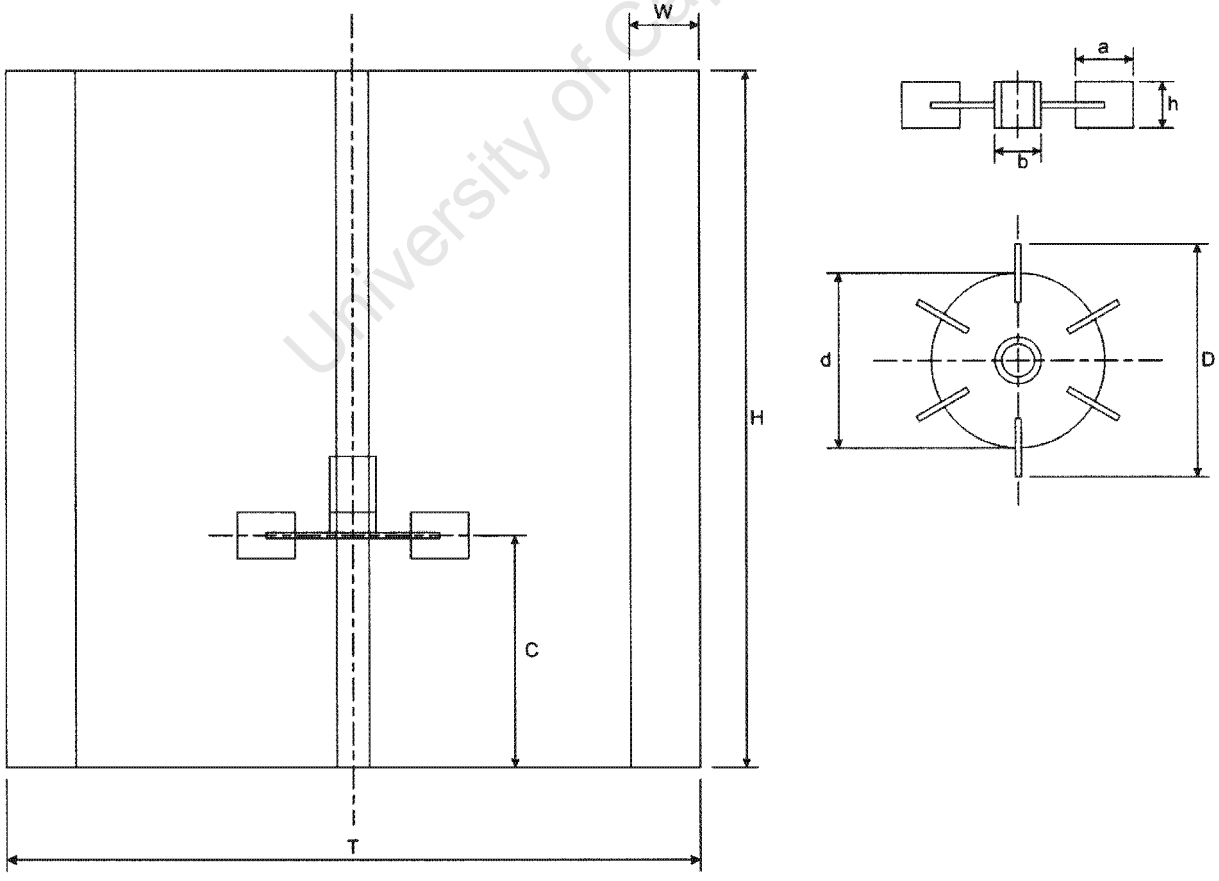

Figure 3.1: Geometric representation of stirred tank

for the multiphase case is depicted in Figure 3.2 and the corresponding spargers are shown in Figure 3.3. The spargers are located at the bottom of the tank and were modelled as four segments.

3.2 MULTIPHASE SYSTEM

Several numerical approaches have been investigated for the multiphase case, the effect of boundary conditions, the multiphase models, geometry and impeller rotation models. These are described in the following sections.

3.2.1 COMPUTATIONAL MODEL

The flow within the stirred vessel is known to be symmetrical. Thus, in addition to the 360° model, a 180° model was used to simulate the vessel. This method allowed for substantial time saving. The Reynolds-averaged Navier-Stokes equations for an incompressible fluid were solved in the commercially available CFD code, FLUENT®.

Impeller Rotation Model

The investigation was based on two impeller rotation models. The Multiple Reference Frames (MRF) model was used for the steady case and the sliding mesh (SM) model for the unsteady case. This was achieved with the definition of two zones, namely the bulk zone and the impeller zone as shown in Figure 3.2. The impeller zone, which contains the region of flow periodicity (Lee and Yianneskis, 1994), was such that it was 1.5 blade height above and below the impeller blade and half the impeller diameter away from the impeller.

Discretisation scheme and Pressure-Velocity Coupling

The QUICK scheme was used for the discretisation of the momentum equations and the volume fraction. Turbulent kinetic energy and dissipation rate were discretised with first order schemes, since the extra computational expense required on higher order discretisation scheme was not justified Engelbrecht (2006). The discretised equations were used to derive pressure and pressure correction (or both) equations to enforce mass conservation at each iteration (or time step) (Ranade, 2002). The phase-coupled SIMPLE algorithm was used for the Eulerian model and the PISO algorithm, which is highly recommended for transient flow calculations (Fluent Inc), for the mixture model.

Computational Grid

The computational grid plays a significant role in the accuracy and stability of the numerical computation. Thus, a fully structured, non-uniform grid with hexahedral body-fitted control volumes was created. Figure 3.4 shows the grid used when the impeller rotation speed was set at 940 rpm. The grid was non-uniform in cell size, with a finer mesh in the impeller discharge region due to the occurrence of a higher degree of turbulence. The higher grid resolution in this large periodicity region helped to reduce numerical diffusion that could lead to the poor prediction of turbulence parameters.

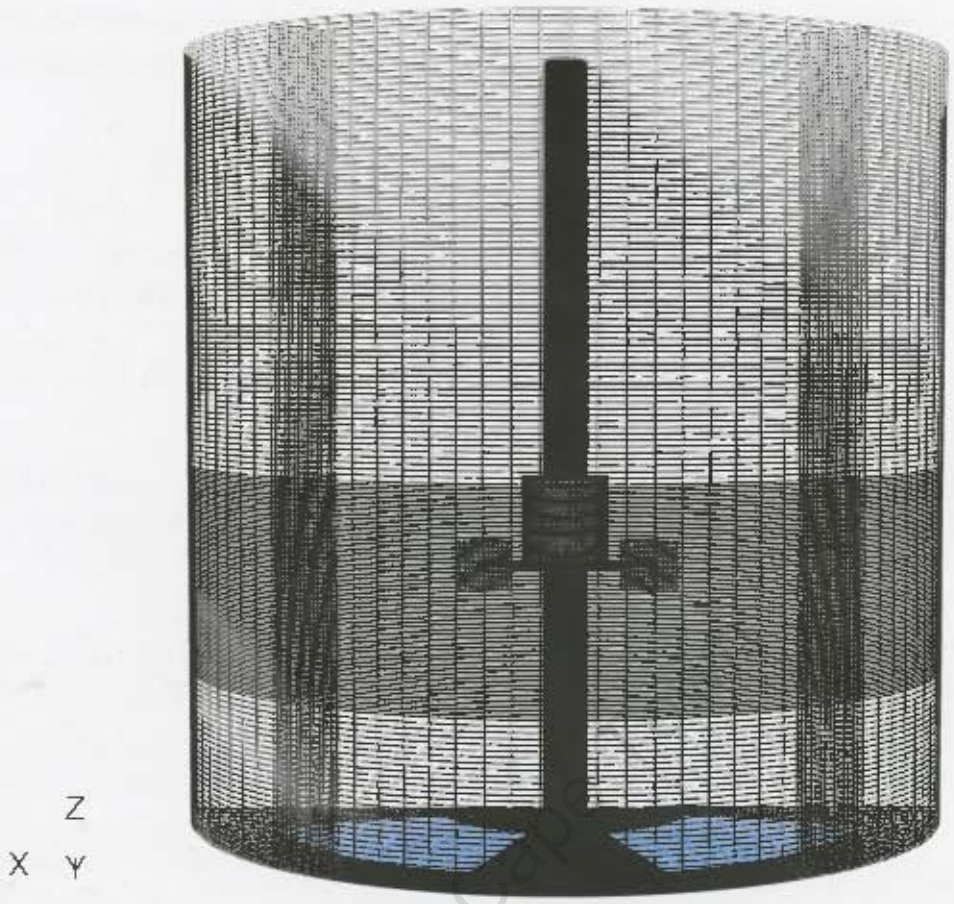

Figure 3.4: Computational Grid for MRF model

The control volume distributions for the different cases are tabulated in Table 3.3. These were for the multiple reference frames model (MRF) and the sliding mesh (SM) for the different rotational speeds. The regions defined corresponds to the same regions represented in Figure 3.2. A finer grid resolution was used at higher impeller speeds due to the smaller bubble size as shown in Table 3.5.

Table 3.3: Computational grid

Impeller Speed (rpm)	Number of Cells			
	Bulk	Impeller	Air Section	Total
630 (SM)	566 400	122 880	277 200	**966 480**
940 (SM)	707 136	183 552	450 240	**1 340 928**
940 (MRF)	333 660	135 090	231 000	**699 750**
1260 (SM)	923 040	455 520	554 400	**1 932 960**

The grid size was limited to the size of the bubble used for the different conditions. This is due to the fact that bubbles are treated as a dispersed phase in each cell, and that the bubble and the fluid encapsulating the bubble form a continuum. For the dispersed $k-\varepsilon$ model, the influence of the primary phase is more significant than that of the secondary phase. Therefore, by using bubbles of a smaller size than the grid

spacing, the effect of the secondary phase on the flow field is minimised and numerical instability avoided.

3.2.2 MULTIPHASE AND TURBULENCE MODEL

The gas-liquid flow regime was simulated with two different models, namely the two-equation Euler-Euler model and the mixture model. The Euler-Euler model has been the most widely used model for various research studies for the modelling of gas-liquid flow (Khopkar et al., 2005; Aubin et al., 2004; Morud and Hjertager, 1996; Ranade and Deshpande, 1999; Ranade and Akker, 1994; Gosman et al., 1992; Engelbrecht, 2006). The standard $k-\varepsilon$ turbulence model of Launder and Spalding (1974) was used to account for the turbulent flow regime. However, the dispersed $k-\varepsilon$ model was used for the Euler-Euler model.

3.2.3 DRAG MODEL

Frothers, a type of surfactant, are generally added to modify bubble properties to reduce coalescence for the generation of a dispersion of small bubbles (Zhang et al., 2003). A higher stability is achieved with the decrease in surface tension of the bubble upon addition of the frother. Thus, the presence of frothers has a drastic effect on the motion of bubbles in a flotation system (Zhou et al., 1993) and consequently the gas hold-up. The experimental work was based on the frother used by Deglon (1998), namely, MIBC, Methyl Iso Butyl Carbinol.

Theoretial Approach

The study presented by Zhou et al.(1993) investigated the effect of the average bubble rise velocity in bubble swarm system. Among the various findings, they reported that at least two main parameters contributed to the reduction of the bubble rise velocity and the increase of gas hold-up. They were the bubble size and the contamination factor.

They presented two sets of data comprising both of an experimental and a theoretical approach based on the following equation:

$$U_{ba} = J_g + \left\{ \frac{A[(1+3.36C_cR_v^2)^{0.5}-1]^2]}{(2C_cR_v)^2} \right\} \frac{(1-k_g\varepsilon_g)^2}{1-(k_g\epsilon_g)^{5/3}} - J_l \tag{3.1}$$

where
- U_{ba} is the average bubble velocity
- J_g is the superficial gas velocity
- J_1 is the superficial liquid velocity
- k_g is the gas hold up coefficient
- C_c is the contamination factor
- R_v is the radius of bubble

where A is given by:

$$A = g\left(\rho_l - \rho_g\right)/(9\mu) \tag{3.2}$$

The experimental and predicted results both showed that addition of frothers gave rise to a decrease in the bubble rise velocity. This can be translated in an increase in the drag coefficient of the bubble.

Thus, in order to reach a higher gas hold-up value, the motion of the bubble can be slowed, by modifying the standard correlation of Schiller and Naumann (3.3):

$$f = \frac{C_D Re}{24} \tag{3.3}$$

where

$$C_D = \begin{cases} 24\left(1 + 0.15Re^{0.687}\right)/Re & Re \leq 1000 \\ 0.44 & Re > 1000 \end{cases} \tag{3.4}$$

Since the flow within the vessel normally has a relative Reynolds number less than 1000, only the first part of the equation was modified in view of increasing the drag coefficient. Thus, based on the data presented by Zhou et al.(1993), the constant 24 was altered to a parameter C. The modified equation is given by:

$$C_D = \frac{C\left(1 + 0.15Re^{0.687}\right)}{Re} \tag{3.5}$$

where C is a model parameter

Based on the study carried out by Zhou et al.(1993), where a maximum 60 ppm of MIBC was used, the experimental and empirical data resulted in a 41% and 71% increase respectively. The parameter C, which included the increase, was used to account for the change.

3.2.4 PHASES AND PROPERTIES

The density and viscosity of the liquid water and the air sparged into the tank is given in Table 3.4. The gas was pumped into the tank at a constant flowrate of 400 $ml.min^{-1}$.

Table 3.4: The fluid properties

Property	**Density** $(kg.m^3)$	**Viscosity** $(kg.m^{-1}.s^{-1})$
Water	998.2	1.003×10^{-3}
Air	1.225	1.78943×10^{-5}

The numerical work was based on single bubble size models. This approach was similarly used by Ranade and Van Den Akker (1994), Ranade and Deshpande (1999), Deen et al. (2002), Khopkar et al. (2005), Kerdouss et al. (2006) and Engelbrecht (2006). The bubble diameter which varied according to the impeller speed is as tabulated in Table 3.5. The diameters used were based on the experimental work presented by Deglon (1998).

Table 3.5: Bubble size diameter

Impeller Speed (rpm)	**Bubble Diameter** (mm)
630	0.38
940	0.2
1260	0.16

3.2.5 PRESSURE HEAD

The surface with atmospheric pressure was modelled by setting the gauge pressure at the outlet to zero. The pressure head within the tank was accounted with the inclusion of the body force due to gravity.

3.2.6 CONVERGENCE CRITERIA

The convergence is dictated by how closely each discretised equation is balanced. The residual, which is the sum of the imbalance in the governing equations over all computational cells in the solution (Ranade, 2002), is used to specify the convergence criteria. Thus, to obtain an acceptable degree of convergence, which is problem dependent, the residuals should be adequately low. For this problem, the convergence criterion for continuity was reduced to a maximum of 1×10^{-3}.

3.2.7 BOUNDARY CONDITIONS

The closed set of governing model equations are solved by defining appropriate initial conditions and boundary conditions. Thus, the solution isolates the system being modelled from the surrounding environment. However, the effect of the environment on the flow field is represented by suitable formulation of boundary conditions, so that, the physical phenomenons within the vessel are simulated properly. Therefore, the boundary conditions were defined as followed:

Wall Boundaries

The standard wall function as proposed by Launder and Spalding (1974) was used to account for the viscous flow regime near the solid surfaces.

Spargers and Outlet Boundary

Literature available to date, shows different approach to model spargers and the outlet of the stirred tank. Ranade and Deshpande (1999) modelled the introduction of gas with mass sources for the gas phase, specified at the sparger cells. The author, (Ranade, 2002), also presented a technique used for bubbles column where the inlet conditions can be specified such that the gas entering the system in form of bubbles can be modelled. This is performed by setting the gas velocity at the sparger inlet equal to the estimated bubble rise velocity. The volume fraction is specified according to the gas volume flow rate. Thus, velocity at inlet and the corresponding volume fraction are given by:

$$V_G = V_{b\infty} \tag{3.6}$$

and

$$\alpha_G = \frac{\langle U_G \rangle}{V_G} \tag{3.7}$$

where V_G is the velocity of gas at inlet
$V_{b\infty}$ is the bubble rise velocity
α_G is the volume fraction of gas at inlet
$\langle U_G \rangle$ is the superficial gas velocity

Mass sinks were specified for the top-most cells to simulate gas exit from the liquid pool. This approach has also been used for various research studies, namely Lane et al. (2002), Khopkar et al. (2005), Spicka

et al. (2001).

Gentric et al (2005) also used a mass source term for the gas inlet. However, the top boundary was modelled as a degassing boundary. That is, an outlet for the gas phase and a no-slip wall for the liquid phase.

The sparger was also modelled as velocity inlets (Morud and Hjertager, 1996; Kerdouss et al., 2006; Engelbrecht, 2006). The velocity was based on a given flowrate. This ensured that there were no outflow of gas or liquid. The gas outlets were modelled as velocity outlet and were determined on a mass balance based on the specified inlet conditions (Morud and Hjertager, 1996).

Recently, in a research study conducted by Engelbrecht (2006), a similar technique as presented by (Ranade, 2002) was used to model the inlet; that is a velocity inlet was used at the sparger. However, the author used an outflow boundary for the outlet. The outflow boundary ensures that the upstream flow is not affected since the flow variables at the boundary are extrapolated within the domain (Fluent Inc). However, no convergence was achieved with this method.

Based on these investigations, for the purpose of the current study the sparger was modelled as a velocity inlet, where the velocity and volume fraction of air were based on the flow-rate used by Deglon (1998), that is 400 $ml.min^{-1}$.

However, for the outlet, three different cases were investigated, where they were modelled as a velocity outlet, pressure outlet and an outflow boundary for the respective cases. The velocity and volume fraction used as outlet condition for the velocity boundary were determined from the mass balance based on the specified inlet conditions. This method ensured that the amount of gas entering the system, leaves at the surface of the tank.

Periodic Boundaries

The extent and size of the solution domain can be reduced by the recognition of the repetitious nature of the fluid flow in a system. The flow within the tank is known to be cyclically repeating in nature. Thus, a 180° model was used in addition to the 360° geometry. This was achieved with the definition rotational periodic boundaries. The periodic boundary ensures that the flow leaving a plane enters a periodically linked plane.

3.3 ANALYSIS

The numerical results for the multiphase system were compared to the experimental work presented by Deglon (1998). The measured data included the mean velocity values, the turbulence parameters, the power draw and the gas hold-up.

The measurement of the velocity components and the turbulent fluctuations are complicated due to the periodic rotation of the impeller causing non-random velocity fluctuations (Wu and Patterson, 1989). There are different approaches presented to date, Wu and Patterson (1989) presented a technique whereby the

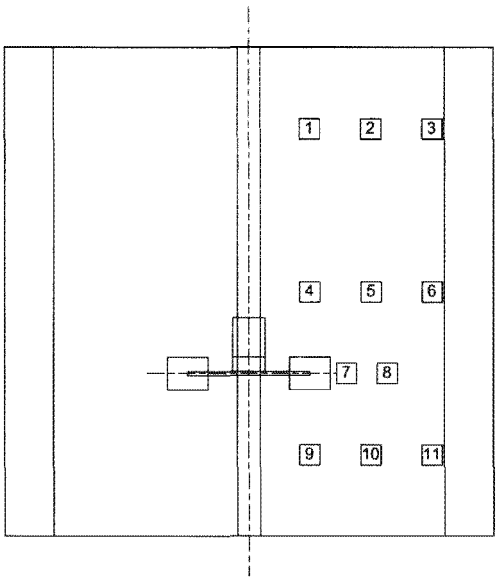

Figure 3.5: Measuring points in stirred tank

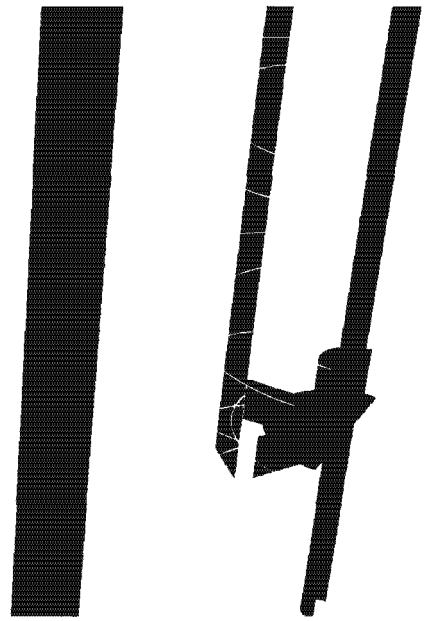

Figure 3.6: Measuring points in computational model

non-dissipating periodic pulsations were removed to obtain meaningful turbulence data. Recently, Engelbrecht (2005) proposed the circumferential averaging and an instantaneous technique for the determination of velocity and turbulence parameters respectively. This method was in good correlation with Wu and Patterson's (1989) work. A similar approach was adopted for the current work for the determination of the velocity and turbulence parameters at the data points as proposed by Deglon (1998). The measuring points are depicted in Figure 3.5.

3.3.1 VELOCITY MEASUREMENT

The velocity at the data points was determined with the circumferential averaging technique. This was performed by creating very fine arcs with a thickness of 0.002 mm of specific radii and heights. Figure 3.6 shows the arcs created for the measurement of the velocity in FLUENT®.

3.3.2 TURBULENCE PARAMETERS MEASUREMENT

The turbulence parameters, comprising of the turbulence kinetic energy and the turbulence energy dissipation rate, were determined using the method proposed by Engelbrecht (2006). Such that, data points denoted by a symbol $\oplus$, as per Figure 3.6 were created at at different heights on a plane midway between any two baffles. Hence, the instantaneous values of the turbulence parameters were determined at the data points as per Figure 3.6.

The predicted R.M.S turbulent velocity was calculated using the k value, given by:

$$u_{R.M.S} = \sqrt{\frac{2}{3}k} \tag{3.8}$$

3.3.3 POWER DRAW

The power draw is the amount of power that must be supplied to the motor to rotate the impeller. This was determined by using the impeller rotational speed and the calculated torque at the impeller.

3.3.4 GAS HOLD-UP MEASUREMENT

The gas hold-up (ϕ) is described as the dimensionless volume fraction of the gas phase in the dispersion and is normally experimentally determined by a volume or area balance performed across a section of a tank (Tatterson, 1991). For the numerical model the gas hold-up was determined from the volume weighted average of air present in the vessel, that is in the impeller zone and bulk zone.

4 RESULTS AND DISCUSSION

The results for multiphase models are presented in this chapter. The predictions for the multiphase models were compared to the experimental data and numerical data presented by Deglon (1998) and Engelbrecht (2006). The numerical data presented by Engelbrecht (2006) showed good correlation to the experimental results reported by Deglon (1998). However, some differences were noted in the prediction of the velocity in the bulk region and the under-prediction of turbulence parameters at the impeller tip. These were attributed to the sampling techniques used by Deglon (1998) as further described in Section 4.1.6. However, both sets of results were used in this investigation for comparative purposes.

The results were compared in terms of the mean velocity, the RMS velocity, the turbulence dissipation rate, the power draw and the gas hold-up. Two main cases were investigated, namely a steady approach and a transient approach. The MRF model with a 180° model was used for the steady state approach, while the sliding mesh with a 360° model was employed for the unsteady simulations. The Euler-Euler multiphase model was used to investigate the discrepancy in the prediction of gas hold-up by using different boundary conditions at the outlet. The transient approach was used to compare the two multiphase models, namely the Euler-Euler model and the mixture model. Based on the findings, the mixture model was used to investigate the effect of changes in the impeller speed upon the fluid flow in the tank. Further investigations were carried to validate the appropriateness of the changes to the Schiller and Naumann drag model in order to account for the effect of frothers.

4.1 STEADY STATE: THE EFFECT OF BOUNDARY CONDITIONS

The multiphase modelling of a basic flow is complex in itself. With the intense hydrodynamics inside the stirred tank the modelling of such flows is more complicated. The steady state model, being computationally less intensive than transient model, is a convenient way to model such flows. However, the prediction of the gas hold-up for gas-liquid systems has been unclear or inadequately predicted for the steady state approach. The convergence criteria were not met in some cases (Engelbrecht, 2006). The first step in this study was to investigate the under-prediction of the gas hold-up and the numerical instability for the steady state scenario at an impeller speed of 940 rpm.

The investigation was based on three cases. An outflow boundary was used for Case 1 and a pressure outlet was used to model the outlet for Case 2. Both models had a volume of air equivalent to half the volume of the tank patched on top of the vessel. This method was used as a degassing medium in order to achieve numerical stability (Fluent Inc). However, this approach was not used for Case 3 where a velocity inlet boundary was used to model the outlet of the tank. This method was used to investigate the effect of the volume of air added on top of the tank on the system. Engelbrecht (2006) reported the inability of the MRF model to result in a model with an acceptable convergence criterion for continuity. It was not clear whether the steep change from the liquid phase to a gas phase could have resulted in the numerical instability or the inherent unsteadiness of the system. This approach was used to better understand the shortcomings of the model in view of developing an acceptable model.

4.1.1 Mean Velocity

The mean velocity for the different regions are tabulated in Table 4.1. The numerical values for the velocity in the bulk region were poorly predicted in the bulk region. However, the velocities at the impeller tip and in the impeller stream showed good correlation to the experimental data. The numerical data compared well to the numerical work presented by Engelbrecht (2006).

Table 4.1: Mean velocity, U ($m.s^{-1}$)

Description	Region		
	Bulk	Impeller Stream	Impeller Tip
Deglon	0.2	0.4	1.6
Engelbrecht	0.039	0.438	1.63
Case 1	0.047	0.495	1.76
Case 2	0.048	0.483	1.77
Case 3	0.048	0.484	1.77

The velocity vectors on a vertical plane midway between the baffles for Case 1 depicted in Figure 4.1.

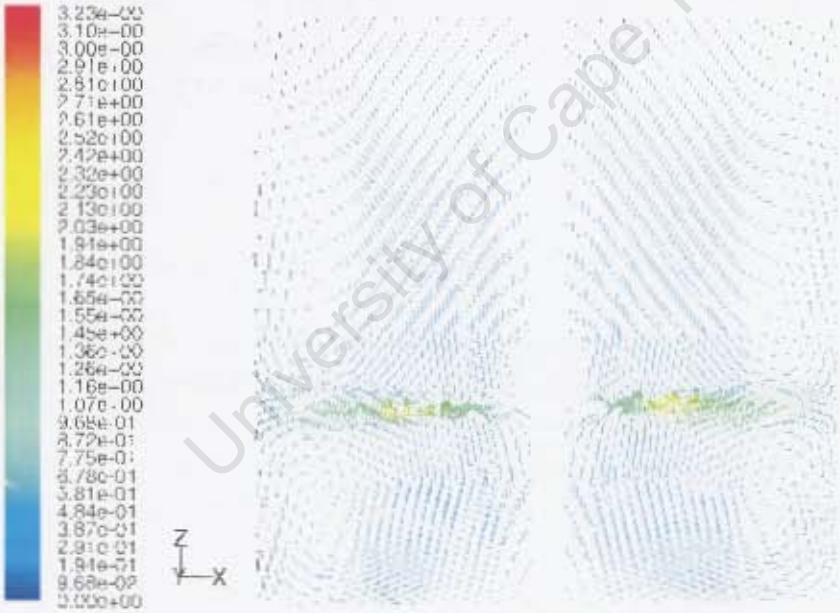

Figure 4.1: Velocity vectors for Case 1

The rotation of the impeller causes the fluid to be drawn upward axially where it is deflected and discharge radially. The resulting jet flows towards the wall of the vessel, splits and is diverted upwards and downwards. The resulting flow which consists of a tangential component is deflected away axially on meeting the baffles. Consequently, two recirculation loops are formed, one below and above the impeller (Kresta and Wood, 1991; Jenne and Reuss, 1991; Ng et al., 1998; Brucato et al., 1998; Hartmann et al., 2004; Newell, 2006). The predicted flow field can be easily recognised in Figure 4.1, with the double structure and the lower and upper recirculation centers. The flow discharge from the impeller can also be observed, with the highest velocity due to the largest effect exerted by the impeller.

4.1.2 Root Mean Square Velocity

The root mean square velocity, $V_{R.M.S}$, for the different regions and cases are tabulated in Table 4.2. The $V_{R.M.S}$ values were slightly under-predicted in the bulk region for all cases. However, at the impeller stream the $V_{R.M.S}$ values were over-predicted and under-predicted at the impeller tip. Similar observations were made by Engelbrecht (2006).

Table 4.2: Root mean square velocity, $V_{R.M.S}$ $(m.s^{-1})$

Description	Region		
	Bulk	Impeller Stream	Impeller Tip
Deglon	0.15	0.25	0.56
Engelbrecht	0.10	0.35	0.29
Case 1	0.12	0.38	0.35
Case 2	0.12	0.38	0.35
Case 3	0.12	0.38	0.36

The contour plot for the turbulent kinetic energy, TKE, on the plane along the impeller disc for Case 1 is shown in Figure 4.2. The expected trailing vortices behind the blades can be clearly observed. The periodicity of the TKE values is easily distinguished, with a minimum at the impeller tip increasing to a maximum in the region between the impeller blades. The decrease in the turbulent kinetic energy away from the impeller due to the decreasing disturbances experienced by the fluid flow can also be seen.

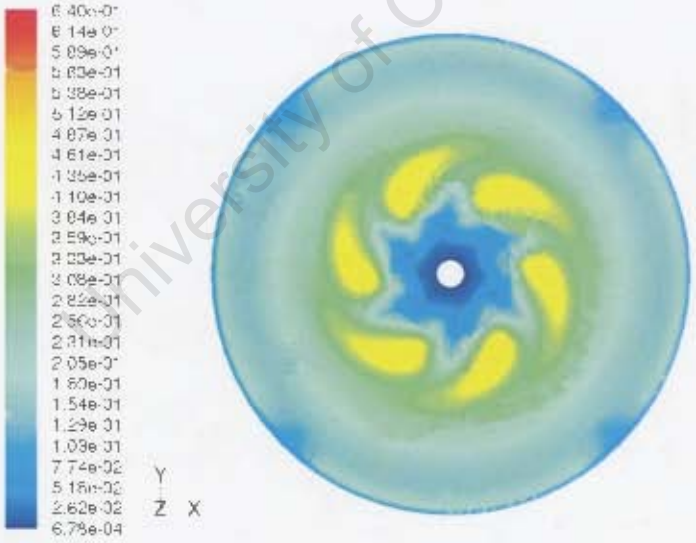

Figure 4.2: Contour plot of turbulent kinetic energy for Case 1

4.1.3 Turbulent Energy Dissipation Rate

The predicted turbulent energy dissipation rate, ε, values in the bulk region showed a poor correlation to the experimental data. The ε values, were reasonably under-predicted in the impeller stream. At the impeller tip, the ε values were considerably under-predicted for all the cases. Similar, trends were observed by Engelbrecht (2006).

Table 4.3: Turbulent energy dissipation rate, ϵ $(W.kg^{-1})$

Description	Region		
	Bulk	Impeller Stream	Impeller Tip
Deglon	0.48	10.5	77.3
Engelbrecht	0.10	10.97	15.25
Case 1	0.17	12.6	20.3
Case 2	0.17	12.5	20.9
Case 3	0.19	12.2	20.9

4.1.4 Power Draw

The results are for the power draw are tabulated in Table 4.4. The experimental results were over-predicted most probably due to the very small amount of gas present in the system.

Table 4.4: Power draw, $(W.kg^{-1})$

Description	Power Draw $(W.kg^{-1})$
Deglon	1.95
Engelbrecht	1.93
Case 1	2.13
Case 2	2.14
Case 3	2.16

However, the predicted power draw showed negligible or no difference for three cases investigated.

4.1.5 Gas Hold-Up

The change of the gas hold-up (ϕ) against the number of iteration for the three cases was plotted as shown in Figure 4.3. It can be observed that the gas hold-up showed a general increase over the 30 000 iterations. After the 30 000 number of iterations, the gas hold-up for Case 1 and 3 were lower than the experimental value of 0.0752. It should be noted that the experimental gas hold-up value is used for comparative purposes only and is not related to the number of iterations. The gas hold-up was over-predicted for Case 2 where a considerable amount of gas was accumulated in the region below the impeller blade.

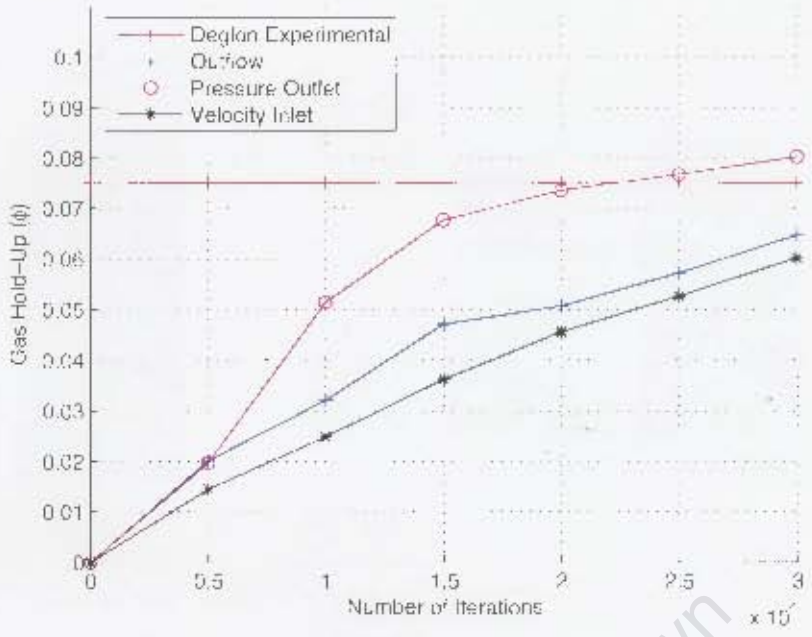

Figure 4.3: Gas hold-up (ϕ) vs number of iterations

The convergence criterion of 1×10^{-3} was not met for Case 1 and 2. Even though convergence was obtained for Case 3, the gas hold-up at that point was under-predicted. However, when the simulation was allowed to run for a further 30 000 iterations, the gas hold-up in the system increased along with the residuals of the continuity. This can be observed in Figure 4.4 where the gas hold-up with the residuals for continuity are plotted over 60 000 iterations.

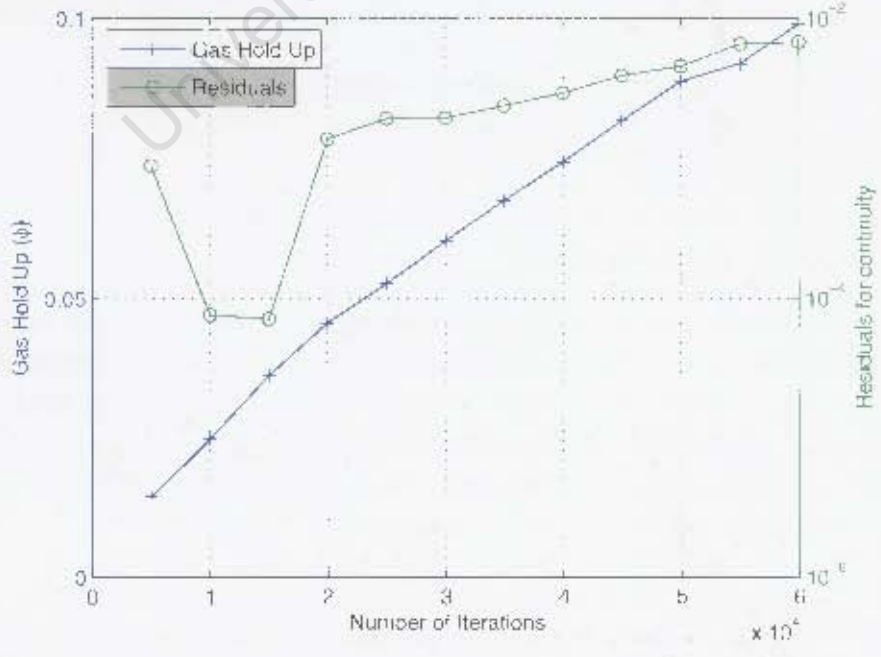

Figure 4.4: Gas hold up (ϕ)/ residuals vs number of iterations

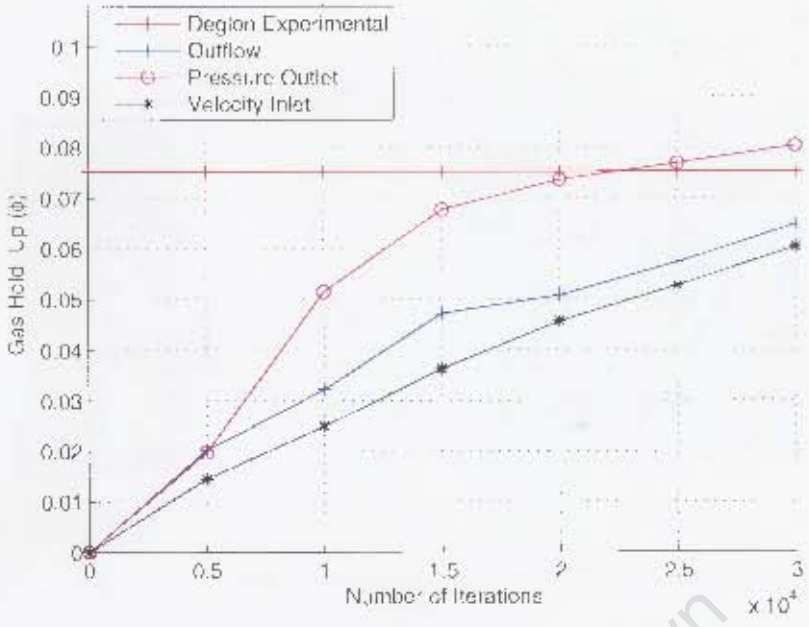

Figure 4.3: Gas hold-up (ϕ) vs number of iterations

The convergence criterion of 1×10^{-3} was not met for Case 1 and 2. Even though convergence was obtained for Case 3, the gas hold-up at that point was under-predicted. However, when the simulation was allowed to run for a further 30 000 iterations, the gas hold up in the system increased along with the residuals of the continuity. This can be observed in Figure 4.4 where the gas hold-up with the residuals for continuity are plotted over 60 000 iterations.

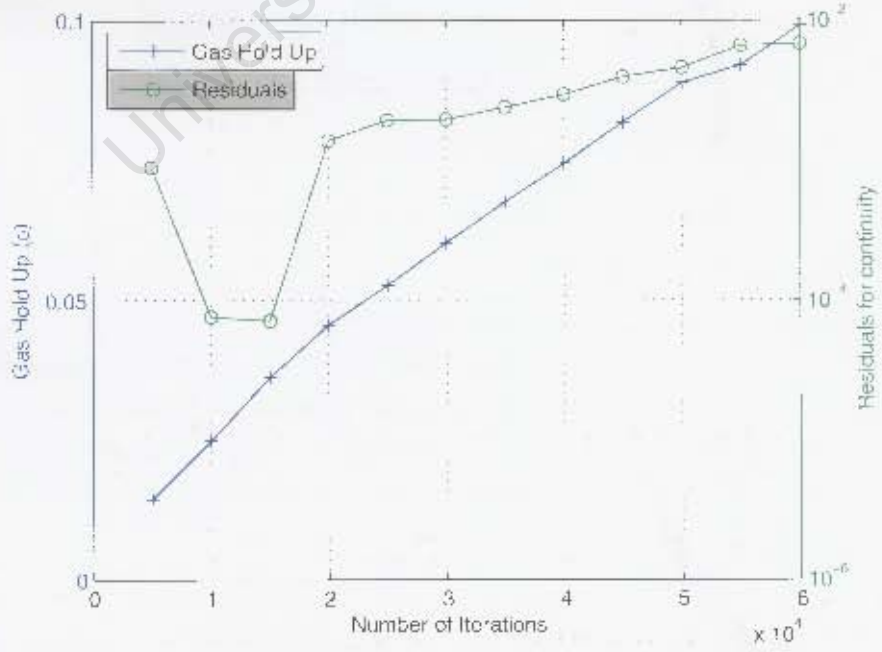

Figure 4.4: Gas hold-up (ϕ) / residuals vs number of iterations

Figures 4.5, 4.6 and 4.7 show contour plots of the volume fraction of air for Case 1, 2 and 3 on a vertical plane.

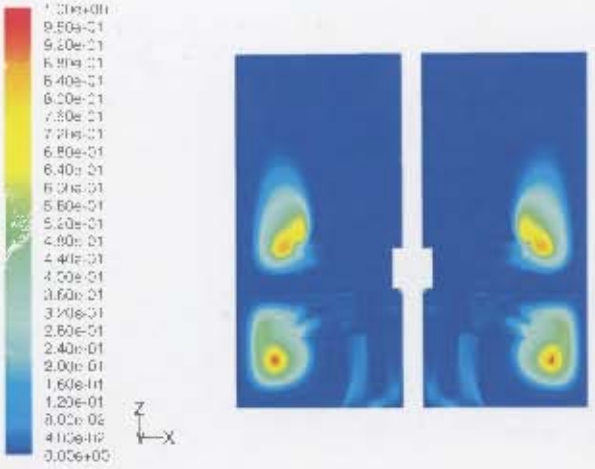

Figure 4.5: Contour plot of volume fraction of air for pressure outlet

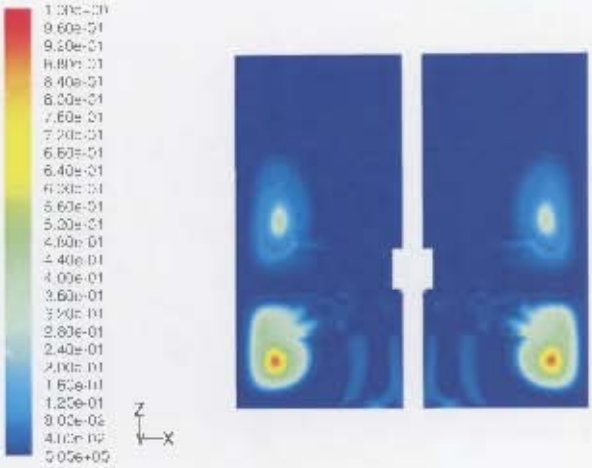

Figure 4.6: Contour plot of volume fraction of air for outflow outlet

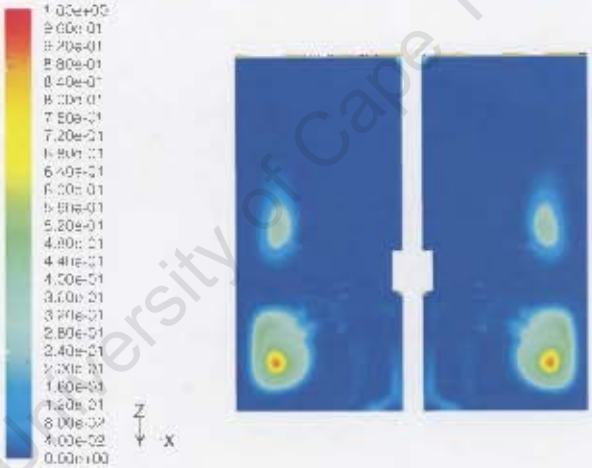

Figure 4.7: Contour plot of volume fraction of air for velocity outlet

The gas distribution was qualitatively well predicted for all cases. The typical flow patterns, including the non-homogeneous gas distributions can be observed. The relatively high accumulation of gas below the impeller due to the occurrence of the lower circulation loop and the lower distribution in the upper section of the tank can be identified. The high concentration of gas at the impeller blade resulting from the suction effect can also be recognised for all cases. The higher gas hold-up for Case 1 can also be seen, with a higher concentration of gas in the two main recirculation loops.

4.1.6 Discussion

The boundary conditions applied to the problem had negligible or no effect on the prediction of the hydrodynamics of the multiphase systems. The Euler-Euler model solves separate set of equations for

each phase. It is probable that the dominant water phase achieved numerical stability within the 30000 iterations. The slight difference in the velocity and turbulence parameters could be due to the different amount of gas in the system with the different boundary conditions. The use of steady state MRF model was found appropriate for the modelling of the hydrodynamics. The 180° model was found appropriate for this study, due to the savings in computational time achieved. The steady state models did not lead to any acceptable result in terms of gas dispersion. The systems were numerically unstable upon introduction of gas. It was not clear whether it was due to the inherent unsteadiness of the system or due to numerical instability of the steady state model. The dominant drag forces could also be one of the reasons. However, no further investigations were made to support this claim.

Mass balance, that is continuity between the amount of air entering and leaving, was achieved for all the three different cases. The conditions at the outlet with the outflow are obtained through the interpolation of flow field within the system. The flow for the pressure outlet relies on the definition of the pressure at the outlet and velocity is set based on the mass balance. However, the velocity outlet might be risky, mainly due to the fact that the outlet condition might not model the actual system, with the air being forced out of the system. This can be avoided with either a pressure outlet or an outflow boundary. More control can be achieved with the pressure outlet and therefore is more suitable.

Mean Velocity

The prediction of the velocity profile was qualitatively and quantitatively reasonable, with the exception of the bulk region where the velocity was under-predicted. Similar observations were made by Engelbrecht (2006). This discrepancy was attributed to the measurement techniques employed by Deglon (1998), where the electrochemical probe used did not take the direction of the flow in the bulk region, which is not purely tangential, into account.

Root Mean Square Velocity

The root mean square velocity, $V_{R.M.S}$, in the bulk region was slightly under-predicted. However, in the impeller stream it was over-predicted and under-predicted at the impeller tip. This disagreement between the numerical and experimental values could be due to the difference in data sampling methods used. For the experimental work, Deglon (1998) determined the RMS velocity by calculating the integral over all frequencies of the energy spectrum function as given by :

$$\overline{u}^2 = \int_0^\infty E_1(n)dn \tag{4.1}$$

where E_1 is the energy spectrum function
n is the frequency

However, for the current study, the RMS turbulent velocity was calculated from the turbulent kinetic energy according to Equation 3.8.

Turbulent Energy Dissipation Rate

The turbulent energy dissipation rate, ε, was under-predicted in the bulk region. The results in the impeller stream showed good quantitative correlation to experimental data. However, ε values were under-predicted at the impeller tip as similarly reported by Engelbrecht (2006). As presented by the

author, this discrepancy can be due to the sampling technique used. The data point used at the impeller tip, being outside the trailing vortices behind the impeller blades, which might not have captured the periodic component of turbulence. Moreover, the effect of the grid resolution, limited by the bubble size, may be responsible for the under-prediction at the impeller as reported by Deglon and Meyer (2006).

Power Draw

The power draw for all three cases were well predicted. They all showed good quantitative correlation to both the experimental work and numerical work presented by Deglon (1998) and Engelbrecht (2006) respectively. The small difference can be attributed to the difference in amount of gas in the system which could have led to some numerical inaccuracies.

Gas Hold-Up

The gas hold-up for all three cases were qualitatively well predicted. However, after 30000 iterations the gas hold-up values (quantitatively) in none of the three cases were acceptable. A general increase of the gas hold-up was observed in all the cases with no sign of stabilisation, suggesting a probable accumulation of gas in the tank. Moreover, the convergence criteria of 1×10^{-3} for the continuity was not met using the pressure outlet and the outflow boundary. It was not clear whether it was the volume of air on top of the tank that was causing this instability.

The system with the velocity outlet and no patch of air on top of the tank met the convergence criteria. However, the gas hold-up at convergence was under-predicted. When the system was allowed to run for more iterations, the gas hold-up increased steadily, resulting in an accumulation in the tank and an increase in residuals for continuity. The very small amount of gas at the beginning of the simulation can explain convergence at the beginning of the simulation, that is convergence could have been obtained for the liquid phase rather than the gas-liquid system, since the system was primarily composed of water at the start. This can also explain the increase in residuals for continuity with the increase in gas phase in the tank.

4.2 UNSTEADY STATE: EFFECT OF MULTIPHASE MODEL

Transient models were investigated due to the inability to achieve convergence with the steady state model. A 360° sliding mesh model was used for the simulation of the impeller rotation and a pressure outlet was used to simulate the outlet of the tank. A volume of air, equivalent to half the volume of the tank was added on top of the tank to act as a degassing medium. Initially, the Euler-Euler model and the mixture model were compared, and then based on the findings, the mixture multiphase model was used to investigate the effect of impeller speed and the appropriateness of the drag model. The model was used to account for the effect of frothers as described in Section 4.2.3.

4.2.1 THE EULER-EULER AND THE MIXTURE MODEL

The appropriateness of the mixture model for the prediction of the gas dispersion was investigated. Both cases were started with no air, mainly for comparative purposes. The two cases were then compared to the experimental data and numerical data presented by Deglon (1998) and Engelbrecht (2006) respectively. Two different set of values as reported by Engelbrecht (2006) were used, firstly GHU1 where 0.15% of the experimental gas hold-up was used as initial value and secondly GHU4 where the MRF was used as the initial condition for the sliding mesh model. The results were compared over the first 30 impeller rotations, where convegence criterion of 1×10^{-3} for continuity was met for all cases.

Mean Velocity

In the bulk region the values of the mean velocities as shown in Figure 4.8, for both models were under predicted as similarly observed by Engelbrecht (2006).

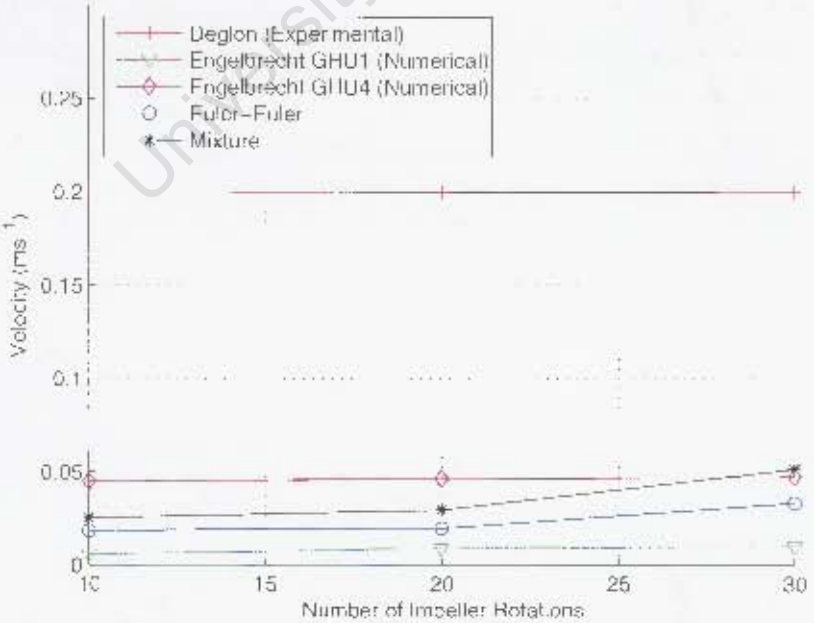

Figure 4.8: Velocity ($m.s^{-1}$) vs impeller rotations in bulk region

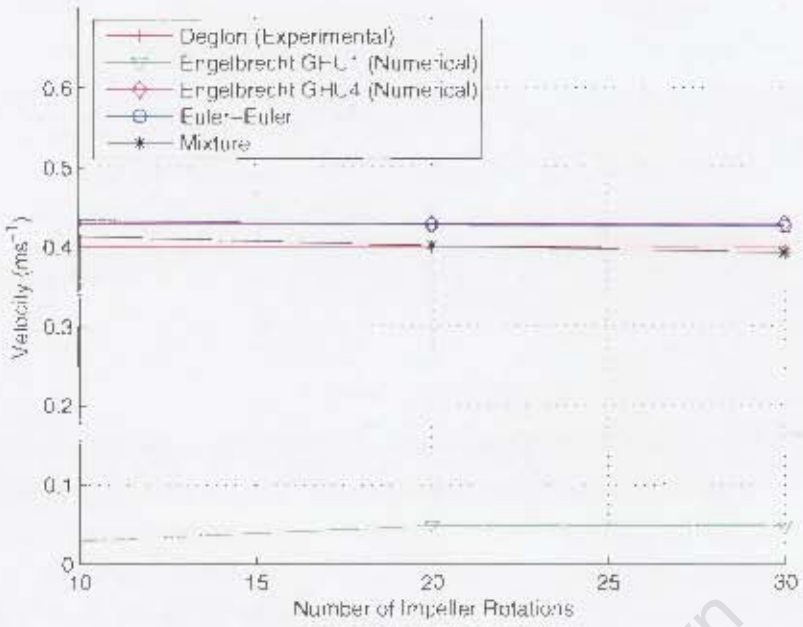

Figure 4.9: Velocity ($m.s^{-1}$) vs impeller rotations in impeller stream

In the impeller stream both models showed good agreement to experimental data. This is observed in the results depicted in Figure 4.9. The values for GHU1 as reported by Engelbrecht (2006) deviated from the current results, even though comparable models were used.

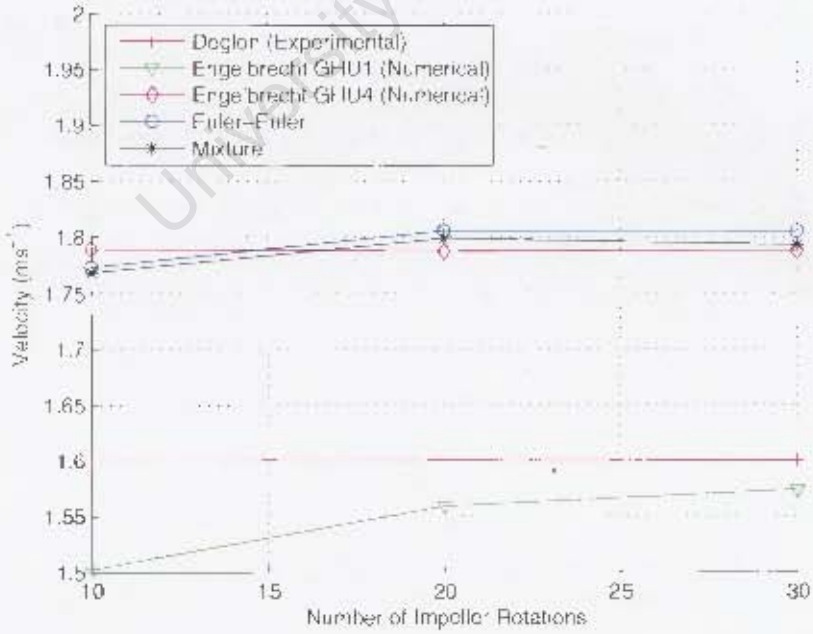

Figure 4.10: Velocity ($m.s^{-1}$) vs impeller rotations at impeller tip

An over-prediction of the mean velocity values was observed for all cases at the impeller tip, except for

the GHU1 case as shown in Figure 4.10 where an under-prediction was observed.

Root Mean Square Velocity

The results for the root mean square velocity values are plotted in Figures 4.11, 4.12 and 4.13 for the bulk region, impeller stream and impeller tip respectively.

The prediction of the $V_{R.M.S}$ values in the bulk region were found to be satisfactory for both models. The values at 30 impeller rotations were comparable to the GHU4 values as reported by Engelbrecht (2006).

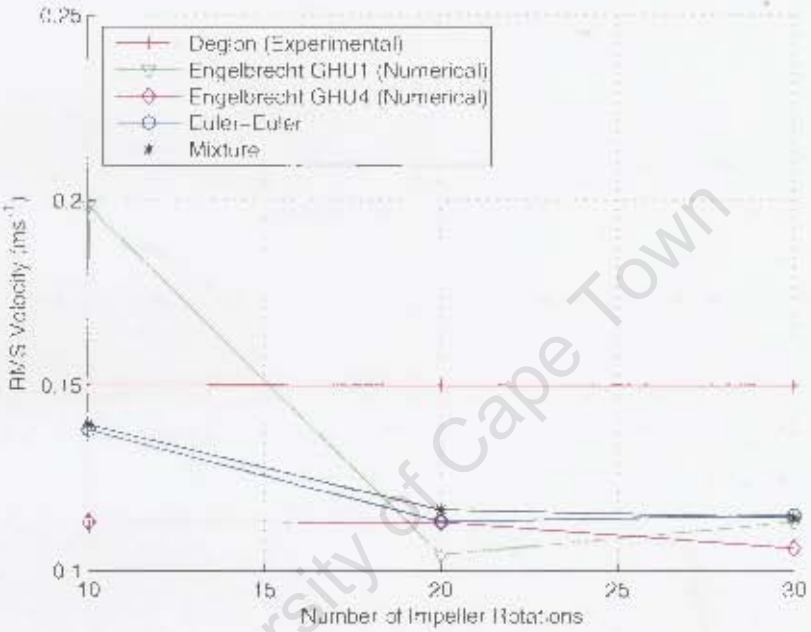

Figure 4.11: $V_{R.M.S}$ $(m.s^{-1})$ vs impeller rotations in bulk region

In the impeller stream as depicted in Figure 4.12, the correlation between the two sets for numerical results were comparable. However, both sets of numerical data over-estimated the experimental results following the trends reported by Engelbrecht (2006) for GHU4.

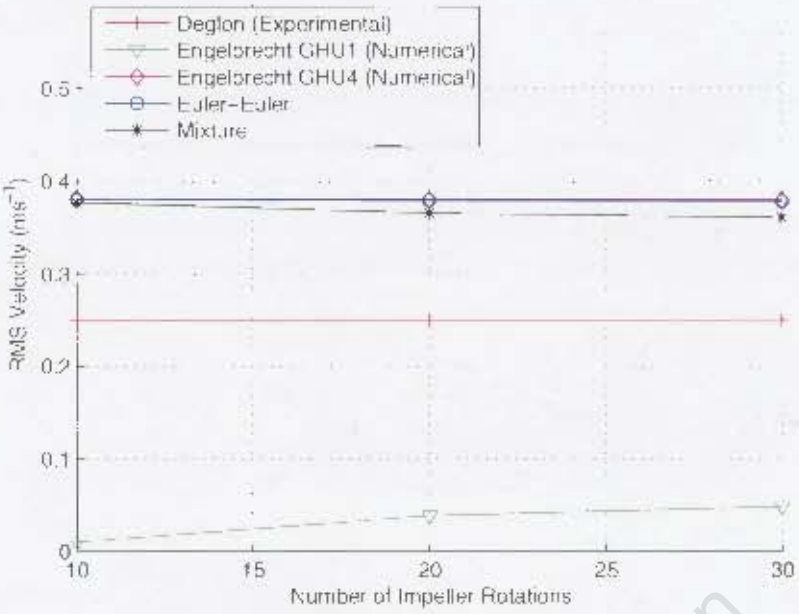

Figure 4.12: $V_{R.M.S}$ $(m.s^{-1})$ vs impeller rotations in impeller stream

However, better predictions were obtained at the impeller tip with the mixture model than with the Euler-Euler model. This is seen in Figure 4.13. The values with the Euler-Euler model were under-predicted. Similar observations were made by Engelbrecht (2006) as described by cases GHU1 and GHU4.

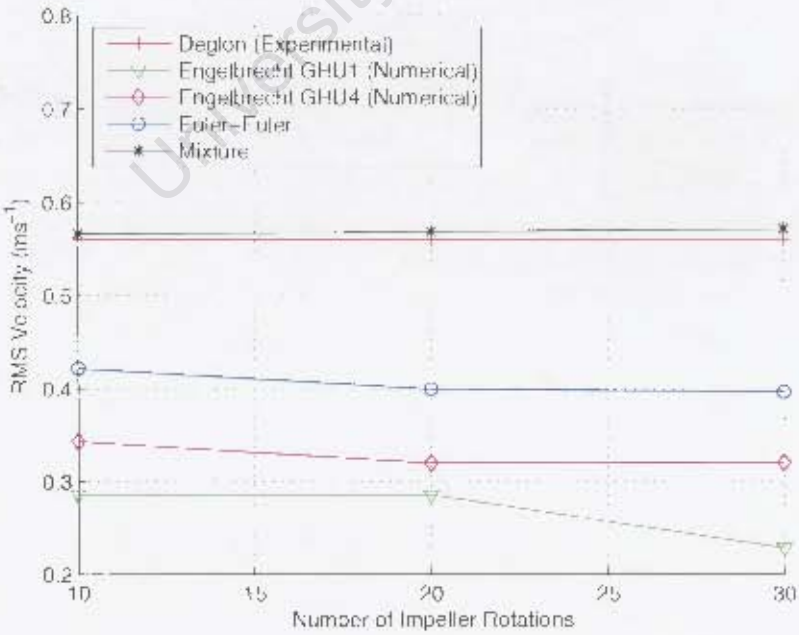

Figure 4.13: $V_{R.M.S}$ $(m.s^{-1})$ vs impeller rotations at impeller tip

Turbulent Energy Dissipation Rate

The turbulent energy dissipation rate for the two multiphase models are shown in Figures 4.14, 4.15 and 4.16.

The turbulent energy dissipation rate values in the bulk for both cases were found to be lower than the experimental value reported by Deglon (1998). The results for the GHU4 case presented by Engelbrecht (2006) showed a similar trend.

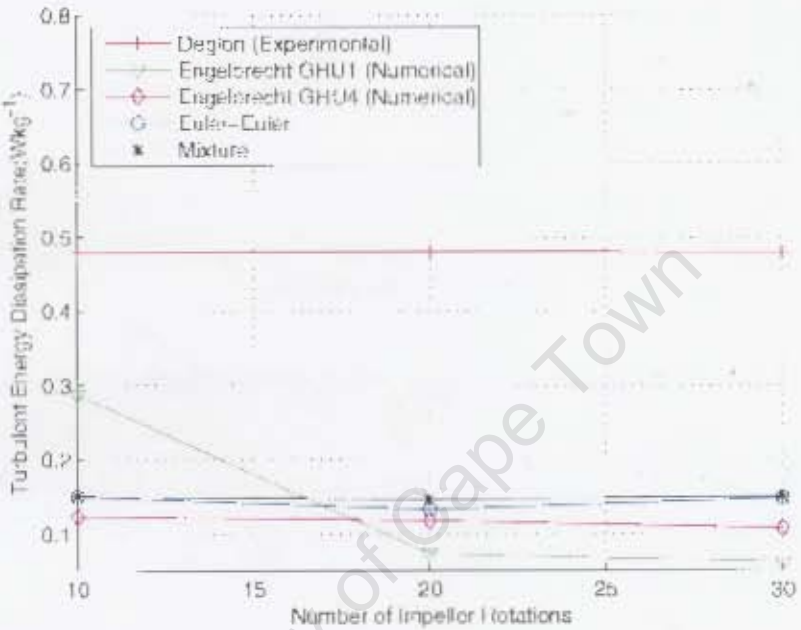

Figure 4.14: Turbulent dissipation rate ($W.kg^{-1}$) vs impeller rotations in bulk region

Even though slightly over-predicted, the values in the impeller stream showed reasonable correlation to experimental data. However, why the results for GHU1 showed an under-prediction of the turbulent energy dissipation rate is unclear.

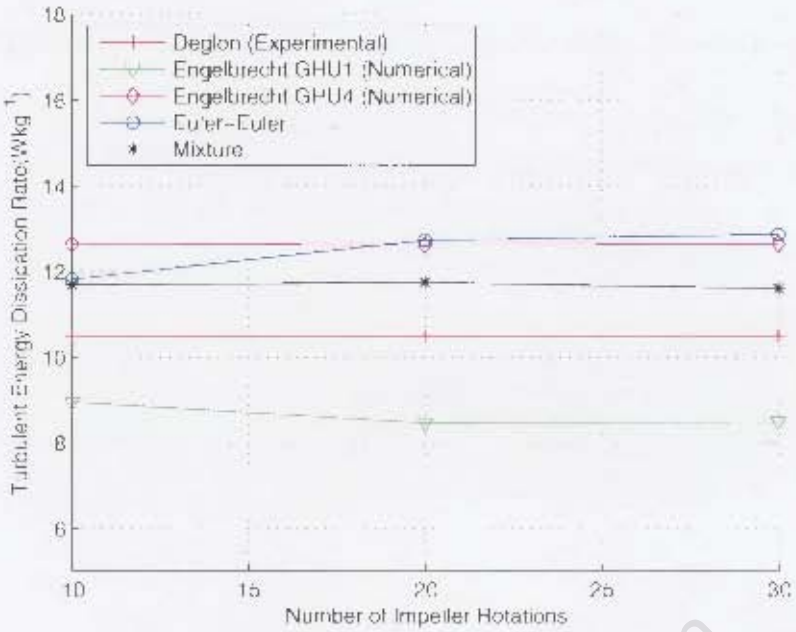

Figure 4.15: Turbulent dissipation rate ($W.kg^{-1}$) vs impeller rotations in impeller stream

At the impeller tip the prediction of the turbulent energy dissipation rate with the mixture model showed good correlation to the experimental data. However, the Euler-Euler model considerably under predicted the turbulence data at the impeller tip as observed by Engelbrecht (2006).

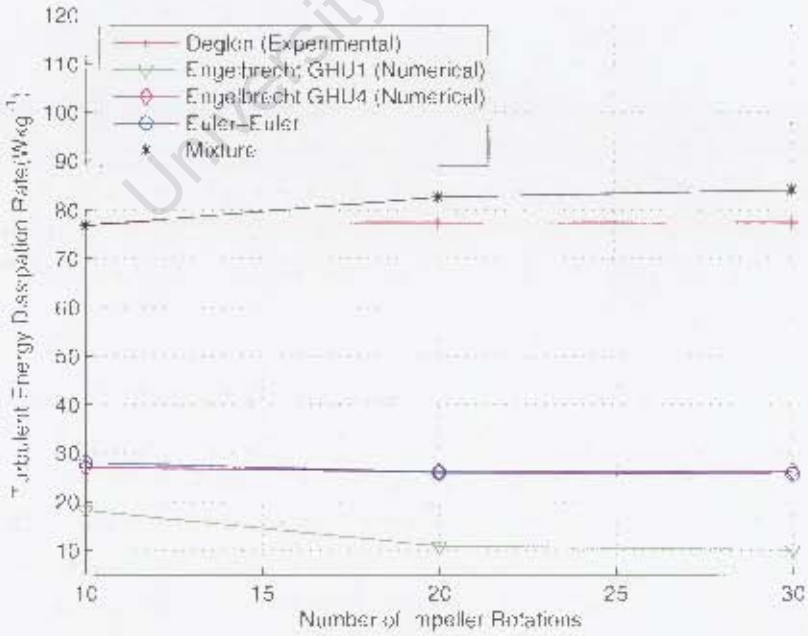

Figure 4.16: Turbulent dissipation rate ($W.kg^{-1}$) vs impeller rotations at impeller tip

Power Draw

The experimental and numerical results for the power draw are as shown in Figure 4.17. Even though a small over-prediction was observed, the power draw for the mixture and the Euler-Euler model were found to be reasonable after 30 impeller rotations. The results presented by Engelbrecht (2006) showed a small deviation from the current values over the first 20 impeller rotations. This difference can be attributed to the amount of gas present at the start of the simulation.

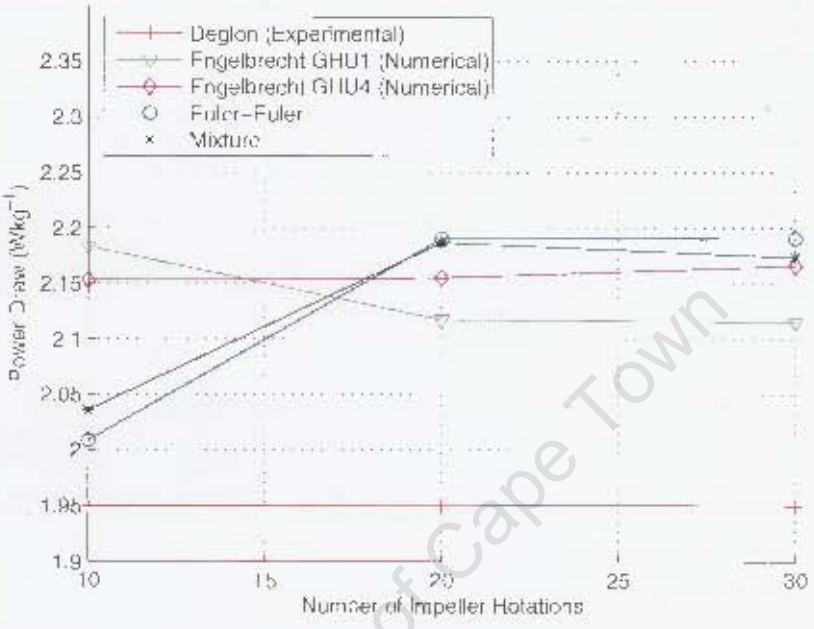

Figure 4.17: Power draw($W.kg^{-1}$) vs impeller rotations

Gas Hold-Up

The prediction of the gas hold-up as expected after approximately 1.9 s was under predicted in all cases. However, the aim of this particular investigation was to look at the appropriateness of the mixture model for the prediction of the gas dispersion. The results are plotted as sampled over the first 30 impeller rotations.

Figure 4.18 showed the gas hold-up for the two models compared to the experimental and numerical work of Deglon (1998) and Engelbrecht (2006). The values for both models were found to increase steadily over the 30 impeller rotations. The gas hold-up for the mixture model was found to be lower than with the Euler-Euler multiphase model. However, after 30 impeller rotations they were found to be comparable. The gas hold-up value obtained for the GHU4 was found to be higher than the values for the current investigation. This was due to the gas accumulated in the tank with the MRF model, which was used as an initial condition for this particular case.

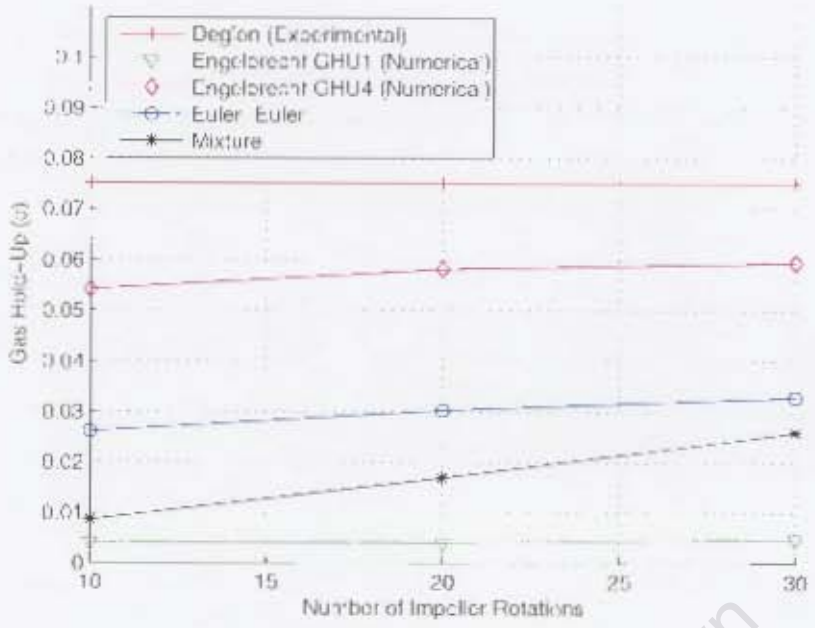

Figure 4.18: Gas hold-up (ϕ) vs impeller rotations

The contour plots of the volume fraction of air for the Euler-Euler and the mixture model over the first 30 impeller rotations are shown in Figures 4.20 to 4.24. The typical gas dispersion distribution in all cases, with the accumulation of air in the recirculation loops below and above the impeller is evident.

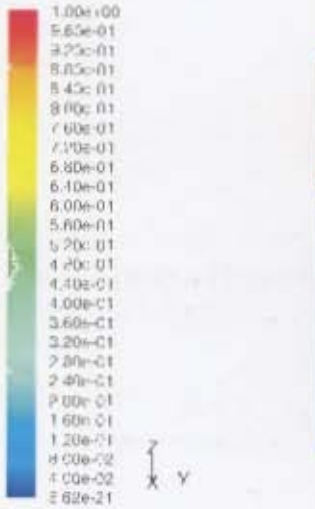

Figure 4.19: Contour plot at 940 rpm after 10 impeller rotations with Euler-Euler model

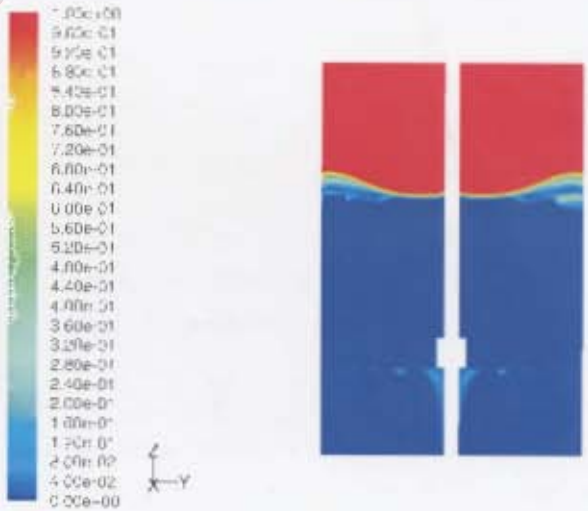

Figure 4.20: Contour plot at 940 rpm after 10 impeller rotations with mixture model

It was also observed that gas first accumulates into the recirculation loops below the impeller and then to the loops above the impeller. The accumulation of gas with the Euler-Euler model was found to be more significant. However, both models were comparable after 30 impeller rotations with regards to the accumulation of air in the recirculation loops.

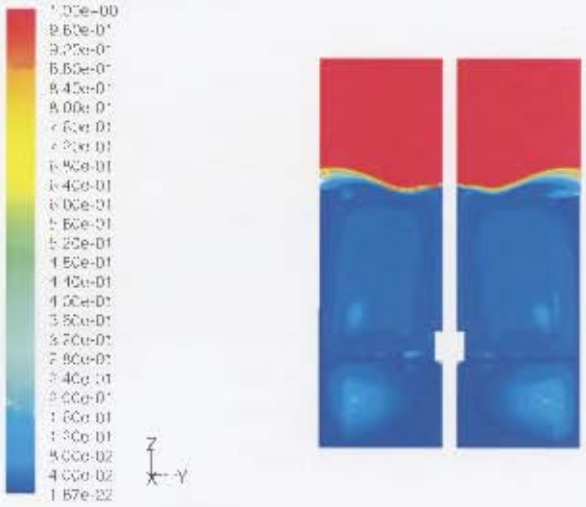

Figure 4.21: Contour plot at 940 rpm after 20 impeller rotations with Euler-Euler model

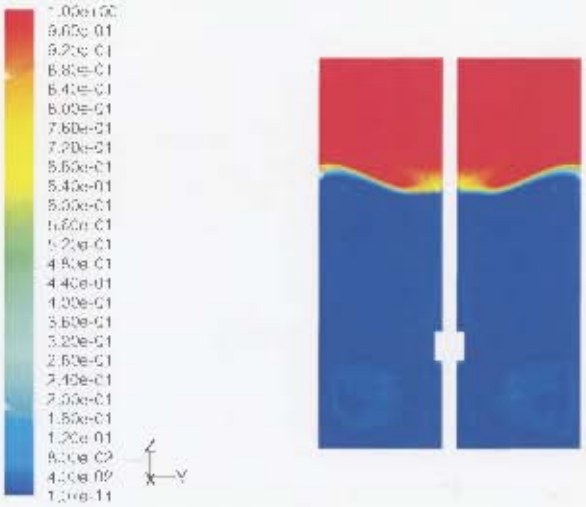

Figure 4.22: Contour plot at 940 rpm after 20 impeller rotations with mixture model

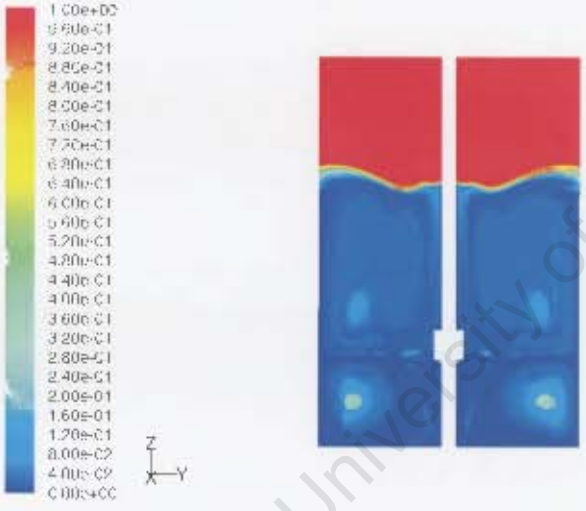

Figure 4.23: Contour plot at 940 rpm after 30 impeller rotations with Euler-Euler model

Figure 4.24: Contour plot at 940 rpm after 30 impeller rotations with mixture model

Even though both models were found to result in an acceptable gas distribution pattern, the gas-liquid interface was poorly simulated. When compared to experimental work presented by Deglon (1998), the water was found to rise to an unrealistic amount above the baffles. This was observed for both models and the discrepancy was found to be exacerbated over time as shown in Figures 4.23 and 4.24 after 30 impeller rotations.

Discussion: Euler-Euler and Mixture Model

The two models were compared over the first 30 impeller rotations, at an impeller speed of 940 rpm. The results showed that the velocity and turbulence parameters predictions were similar for both models. The velocity values showed good correlation to the experimental data, except in the bulk region where the

results were under-predicted. The turbulence parameters obtained were similar in all cases. However, higher values were obtained at the impeller tip for the mixture model. This could be attributed to the difference in turbulence model used. The dispersed $k-\varepsilon$ model was used for the Euler-Euler model and the standard $k-\varepsilon$ for the mixture model. This difference and the high degree of turbulence at the impeller tip could have resulted in the inconsistency at the impeller tip. The poor correlation to the experimental work presented by Deglon (1998) could be attributed to the experimental sampling techniques used as explained in Section 4.1.6.

The comparison of the numerical work presented by Engelbrecht (2006) showed similar trends observed for the two models. The results for the GHU1 model was unclear. A similar approach was used for the current work (started initially with no air) and the GHU1 model where the simulation was started with 0.15% of the experimental gas hold-up. It was observed that different values for the mean velocity and turbulence parameters were under-predicted with the GHU1 model. The author claimed that the flow field was not fully developed for simulations corresponding to GHU1. However, this was unclear as the numerical models with both the mixture model and the Euler-Euler model both showed that the flow is fully developed after 30 impeller rotations. This finding was supported by the comparable results obtained from the steady state models.

The prediction of the power draw was reasonably acceptable when compared to the experimental data. Comparable values to the numerical work presented by Engelbrecht (2006) were observed. The small over-prediction could be due to the small amount of the gas present in the system over 30 impeller rotations, since the power draw is expected to drop with aeration.

The gas hold-up for the two models were comparable. The experimental gas hold-up was under-predicted as expected, since the 30 impeller rotations modelled represented about 1.9 s, compared to the required 30 s required to obtain reasonable gas hold-up values. However, the results showed that both model could be used for the modelling of the gas phase.

The gas hold-up values for the GHU4 case as predicted by Engelbrecht (2006) showed better prediction. This model used the MRF as an initial condition for the sliding mesh model. However, as found from the steady state models, the MRF was not appropriate to model gas dispersion. Therefore, using the MRF as an initial condition might lead to some numerical inaccuracies.

Both models showed some discrepancies in simulating the fluid flow at the gas-liquid interface. A considerable rise in the water level was observed above the baffles. This lead to an unrealistic entrainment of gas inside the tank. At this point it was unclear whether this phenomenon was physically possible or was due to some numerical inability of both multiphase models to correctly simulate the gas-liquid interface. Thus, this discrepancy was further investigated in Section 4.2.2.

4.2.2 Effect of Impeller Speed

The mixture model was used to investigate the effect of impeller speed. The main objective of this section was to investigate the behaviour of the gas-liquid interface upon a change in impeller speed. A 360° model with the sliding mesh model was used to model the rotation of the impeller and the mixture model to model the gas liquid flow. The investigation was based on three impeller speeds, 630 rpm, 940 rpm and 1260 rpm. The results were compared to the experimental results reported by Deglon (1998). These were validated in terms of the velocity values, the turbulence parameters, power draw and the gas hold-up. The numerical data were sampled over the first 30 impeller rotations as reported in the following sections.

Mean Velocity

The mean velocity for the different regions are plotted in Figure 4.25, 4.26 and 4.27. Sets of results were plotted at 10 impeller rotations intervals. The general increase in the mean velocity values was observed in all cases.

The mean velocity values in bulk region, depicted in Figure 4.25, showed an under prediction of the experimental data. An increase in the velocity values was observed over the 30 impeller rotations simulated. This shows that even though convergence is obtained at the beginning of the simulation the flow is not fully developed over the first 20 impeller rotations. The results supports the findings made by Wechsler (1999), reporting that 30 impeller rotations is required to obtain a fully developed flow.

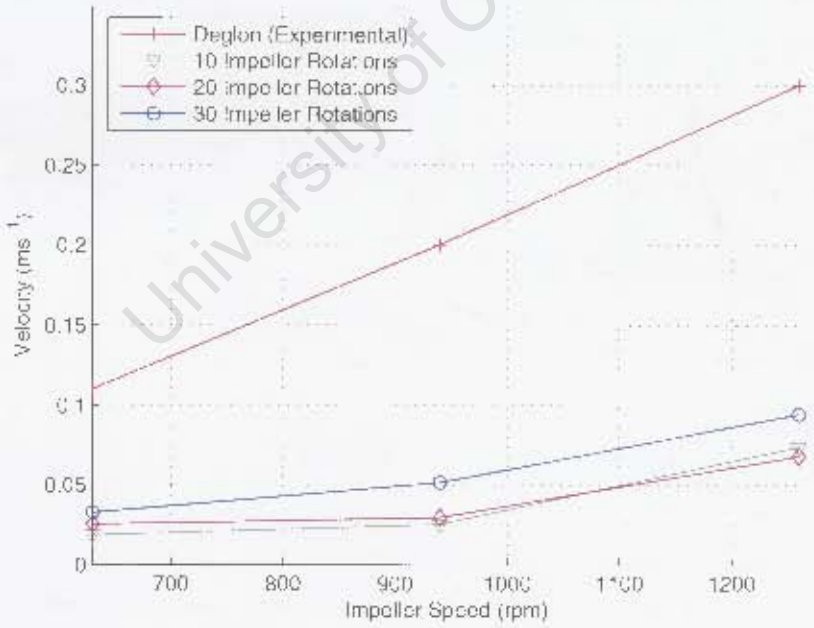

Figure 4.25: Velocity ($m.s^{-1}$) vs impeller speed (rpm) in bulk region

The results at the impeller stream as shown in Figure 4.26 showed good correlation at 630 rpm and 940 rpm. However, the experimental data was under-predicted at 1260 rpm. Similar observations were reported by Engelbrecht (2006) for a single phase case.

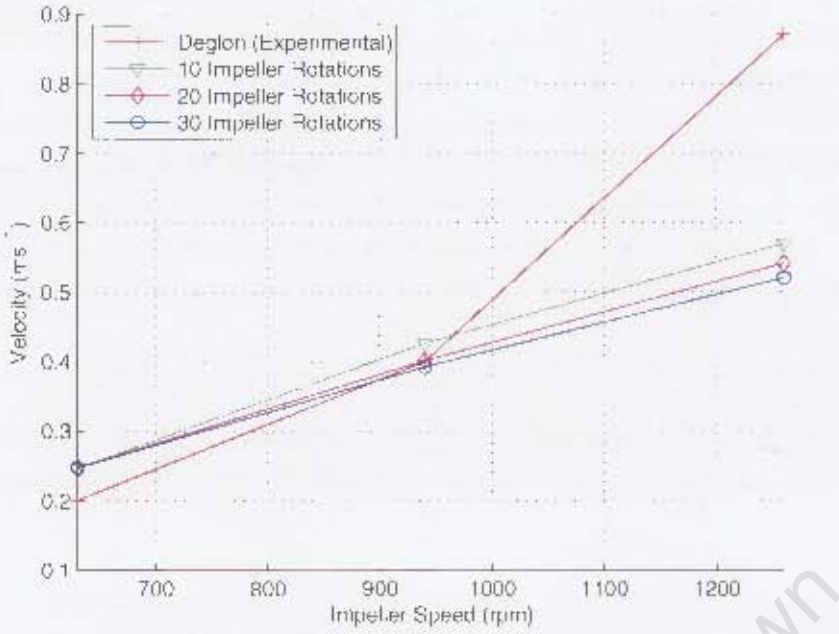

Figure 4.26: Velocity $(m.s^{-1})$ vs impeller speed (rpm) in impeller stream

The velocity values at the impeller tip showed good qualitative correlations but were over-predicted for all cases. The results over the first 30 impeller rotations showed negligible difference, suggesting that the flow in this region attained numerical stability at the impeller tip.

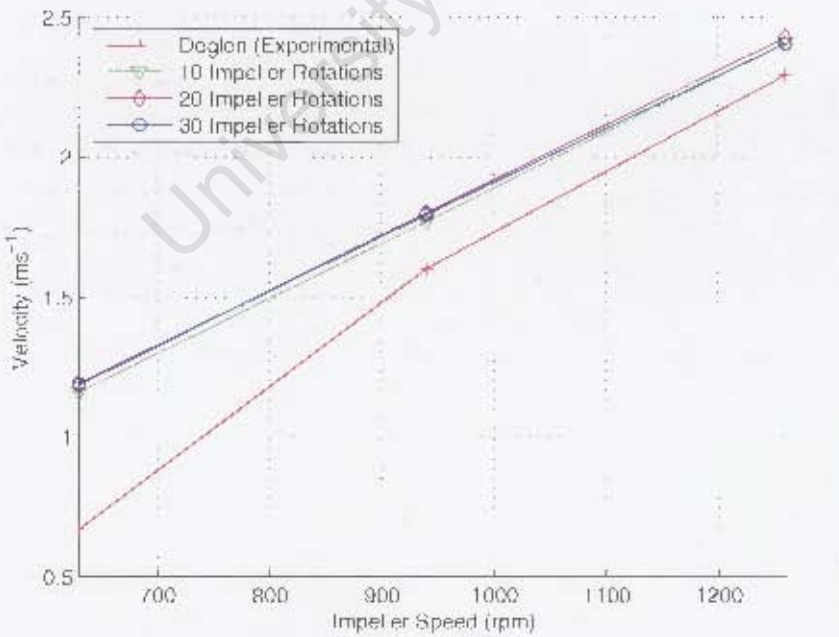

Figure 4.27: Velocity $(m.s^{-1})$ vs impeller speed (rpm) at impeller tip

Root Mean Square Velocity

The numerical results for the root mean square velocity are plotted in Figures 4.28, 4.29 and 4.30. The data showed an increase in root mean square velocity with increasing impeller speed.

The predicted root mean square velocity values in the bulk region is shown in Figure 4.28. The results showed good qualitative correlation to the experimental data. However, the numerical data were under-predicted in all cases. A similar trend was observed by Engelbrecht (2006). It can be also observed that the flow in the bulk region is not fully developed over the first 10 impeller rotations.

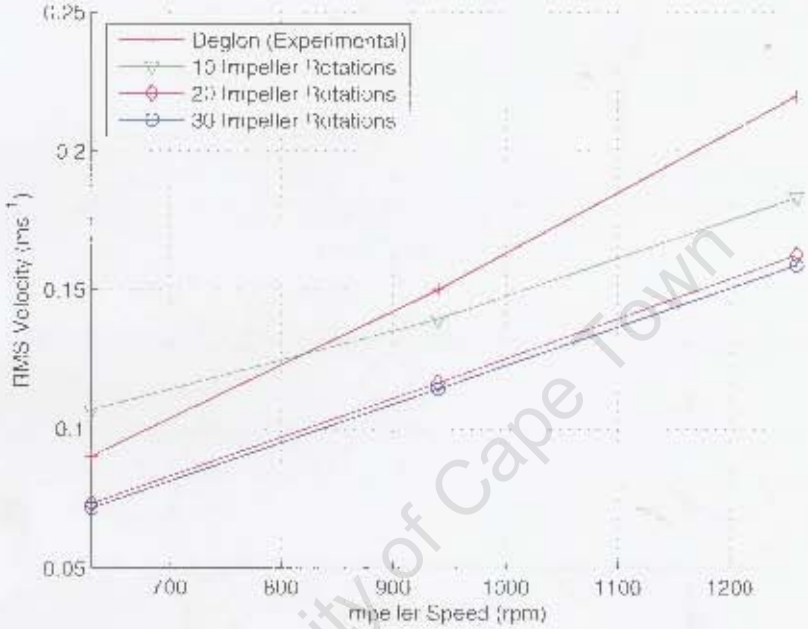

Figure 4.28: $V_{R.M.S}\,(m.s^{-1})$ vs impeller speed (rpm) in bulk region

The numerical data in the impeller stream was over-predicted although similar trends were observed from the experimental results. The discrepancy was more substantial at 630 rpm and 940 rpm with a better correlation at 1260 rpm as shown in Figure 4.29. Similarly, the single phase data reported by Engelbrecht (2006), showed an over-prediction at 630 rpm and 940 rpm but with an under prediction at 1260 rpm.

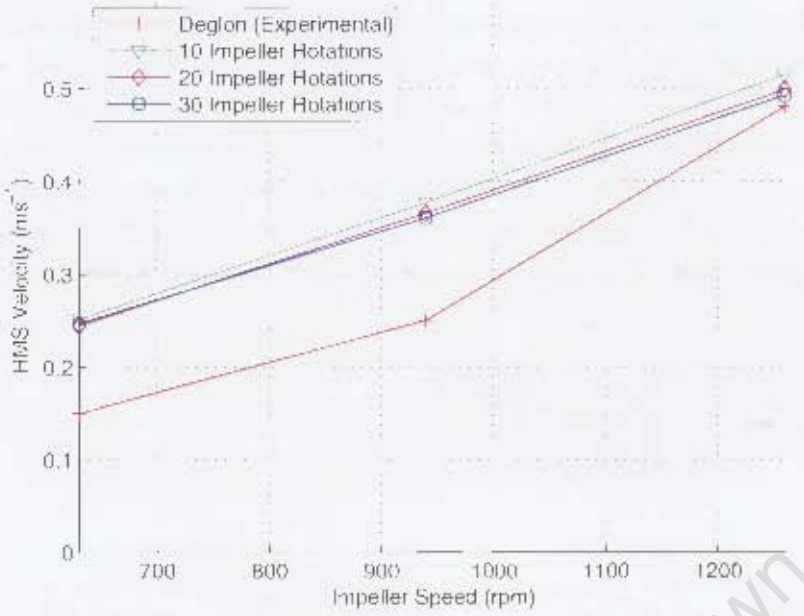

Figure 4.29: $V_{R.M.S}$ $(m.s^{-1})$ vs impeller speed (rpm) in impeller stream

At the impeller tip, the correlation between experimental and the numerical data was qualitatively good but quantitatively poor, with an over-prediction for all cases. The results at the 10 impeller rotations intervals showed similar trends. It can also be observed that that the discrepancy was exacerbated at 630 rpm.

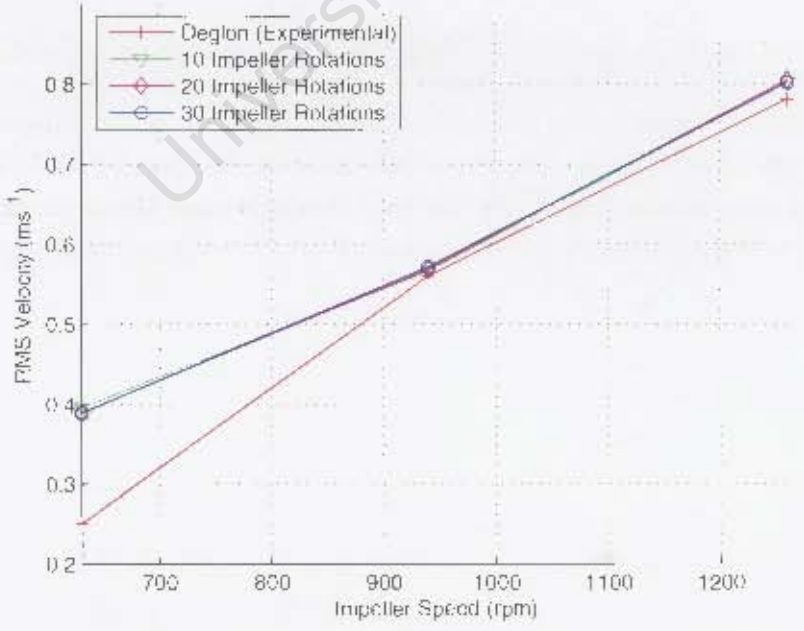

Figure 4.30: $V_{R.M.S}$ $(m.s^{-1})$ vs impeller speed (rpm) at impeller tip

Turbulent Energy Dissipation Rate

The turbulent energy dissipation rates values for the numerical and experimental work for the range of rotational speed investigated are plotted in Figures 4.31, 4.32 and 4.33. The experimental and numerical data showed good qualitative correlation for the different regions.

The results in the bulk region as depicted in Figure 4.31 showed an under prediction of the experimental data, as similarly observed for the mean velocity and root mean square velocity values. However, little or no difference in the energy dissipation rate values is observed over the 30 impeller rotations.

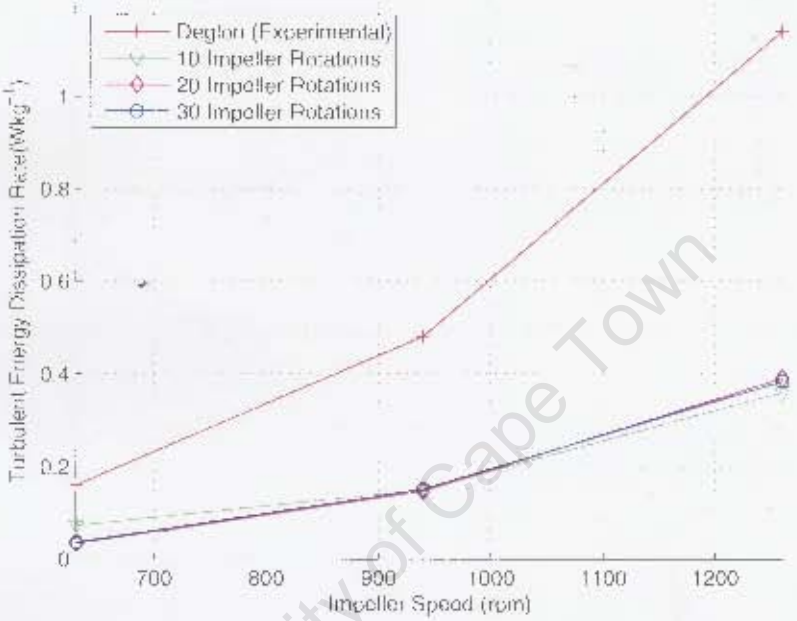

Figure 4.31: Turbulent dissipation rate ($W.kg^{-1}$) vs impeller speed (rpm) in bulk region

In the impeller stream, the ε values as shown in Figure 4.32 were predicted reasonably well at 630 rpm and 940 rpm. However, the numerical results were under-predicted at 1260 rpm. The results for each 10 impeller rotations intervals were similar showing that the flow was most likely fully developed in the impeller region.

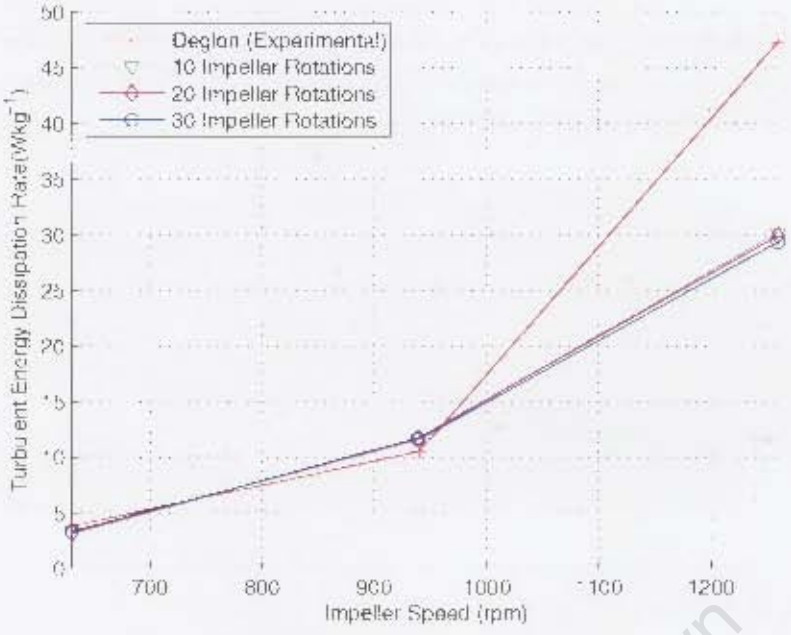

Figure 4.32: Turbulent dissipation rate ($W.kg^{-1}$) vs impeller speed (rpm) in impeller stream

The prediction for ε at the impeller tip were reasonable at 630 rpm and 940 rpm, although over-predicted in all cases. The discrepancy was found to be exacerbated with increase in impeller speed. Similar observations were made in the impeller stream and bulk region.

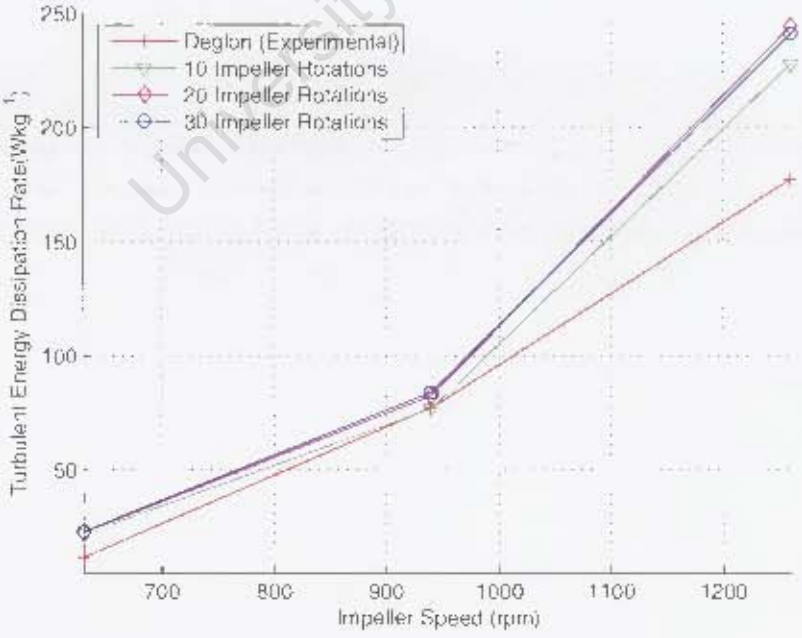

Figure 4.33: Turbulent dissipation rate ($W.kg^{-1}$) vs impeller speed (rpm) at impeller tip

Turbulent Energy Dissipation Rate

The turbulent energy dissipation rates values for the numerical and experimental work for the range of rotational speed investigated are plotted in Figures 4.31, 4.32 and 4.33. The experimental and numerical data showed good qualitative correlation for the different regions.

The results in the bulk region as depicted in Figure 4.31 showed an under-prediction of the experimental data, as similarly observed for the mean velocity and root mean square velocity values. However, little or no difference in the energy dissipation rate values is observed over the 30 impeller rotations.

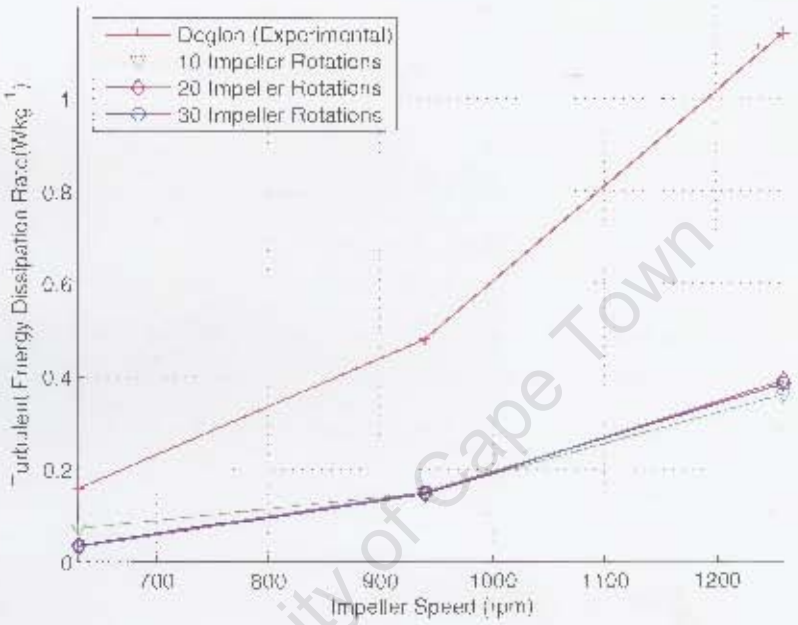

Figure 4.31: Turbulent dissipation rate ($W.kg^{-1}$) vs impeller speed (rpm) in bulk region

In the impeller stream, the ε values as shown in Figure 4.32 were predicted reasonably well at 630 rpm and 940 rpm. However, the numerical results were under-predicted at 1260 rpm. The results for each 10 impeller rotations intervals were similar showing that the flow was most likely fully developed in the impeller region.

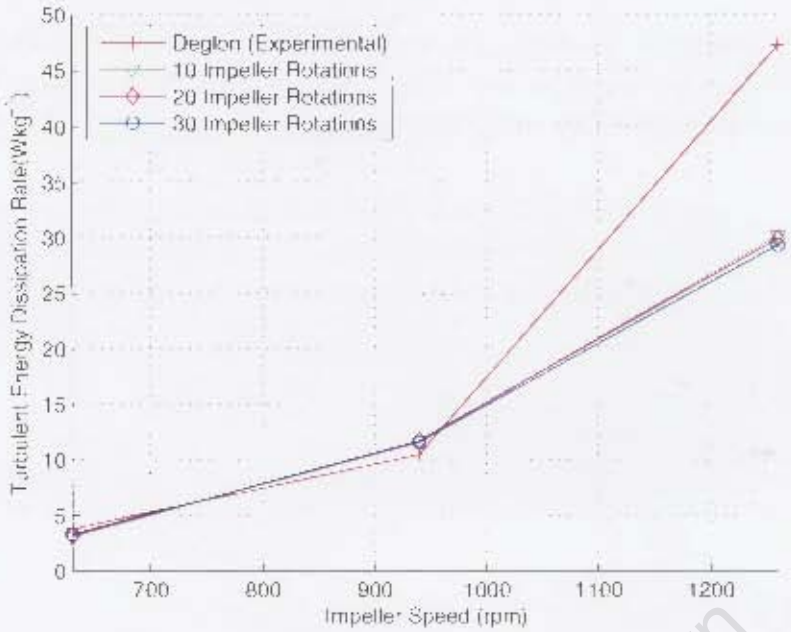

Figure 4.32: Turbulent dissipation rate ($W.kg^{-1}$) vs impeller speed (rpm) in impeller stream

The prediction for ε at the impeller tip were reasonable at 630 rpm and 940 rpm, although over-predicted in all cases. The discrepancy was found to be exacerbated with increase in impeller speed. Similar observations were made in the impeller stream and bulk region.

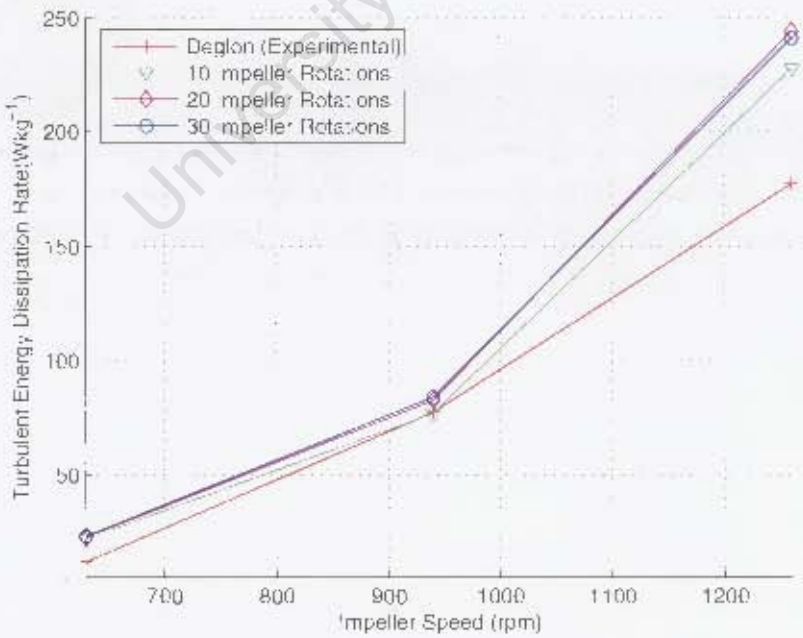

Figure 4.33: Turbulent dissipation rate ($W.kg^{-1}$) vs impeller speed (rpm) at impeller tip

Power Draw

The power draw for the three different impeller speeds over the first 30 impeller rotations is represented in Figure 4.34. The numerical and experimental data correlated well, with an increase in power with an increase in impeller speed. However, the power draw was over-predicted by 15% at 1260 rpm. A similar observation was made by Engelbrecht 2006 with an over-prediction of 5% for a single phase system.

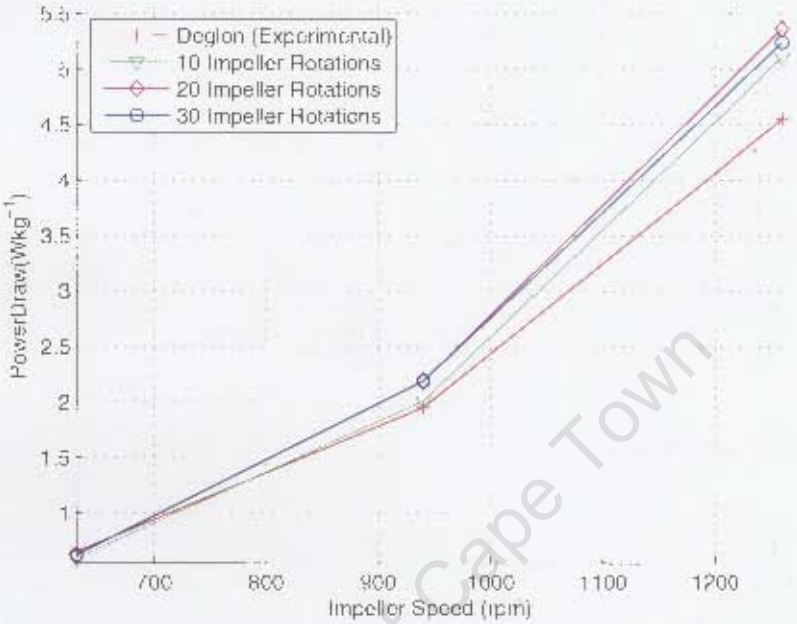

Figure 4.34: Power draw ($W.kg^{-1}$) vs impeller speed (rpm)

Gas Hold-Up

The gas hold-up over the first 30 impeller rotations for the range of impeller speed is shown in Figure 4.35. It is clear that the gas hold-up increases with the impeller speed even though the 30 impeller rotations does not represent the same time interval for all cases. The gas hold-up for all cases were under-predicted due to the relatively short time period over which the system was modelled.

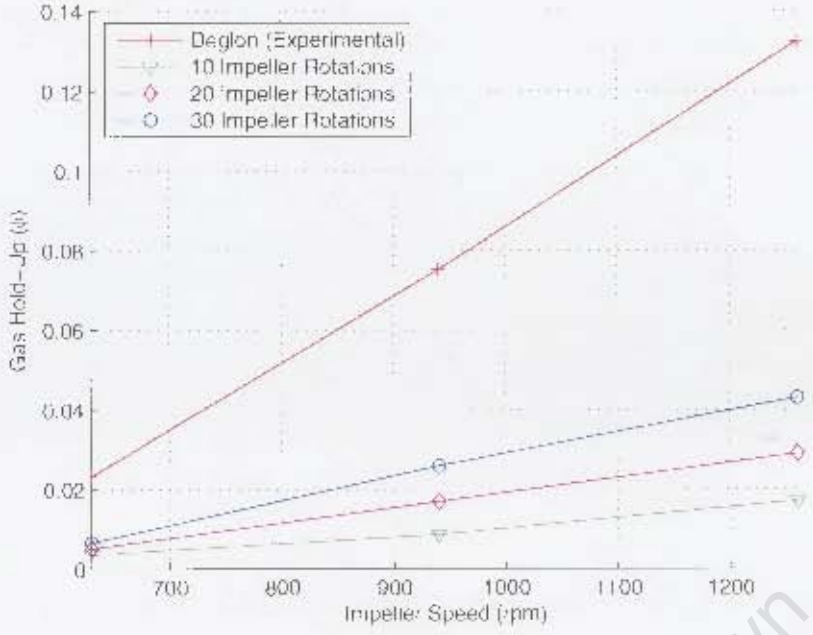

Figure 4.35: Gas hold-up ϕ vs impeller speed (rpm)

Figures 4.36 to 4.41 show the contour plots of the volume fraction of air at 630 rpm and 1260 rpm. The gas dispersion pattern near the impeller was well predicted. The gas-liquid interface however was poorly predicted in both cases. The inaccuracy previously observed at 940 rpm was more substantial at 1260 rpm. The interface after 30 impeller rotations as shown in Figure 4.41 was completely unrealistic. The water level rose by a considerable amount above the baffles and is clearly not physically possible. This showed that the model failed to correctly simulate the water's free surface.

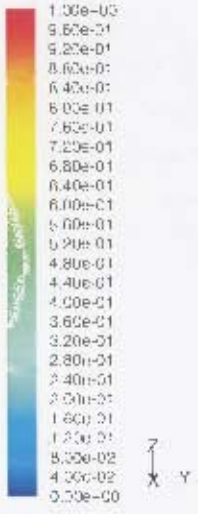

Figure 4.36: Contour plot at 630 rpm after 10 impeller rotations

Figure 4.37: Contour plot at 1260 rpm after 10 impeller rotations

The resulting phenomenon was less substantial at the 630 rpm as shown in Figure 4.40. The entrainment

of gas inside the tank was very small with the small increase in the water level above the baffles.

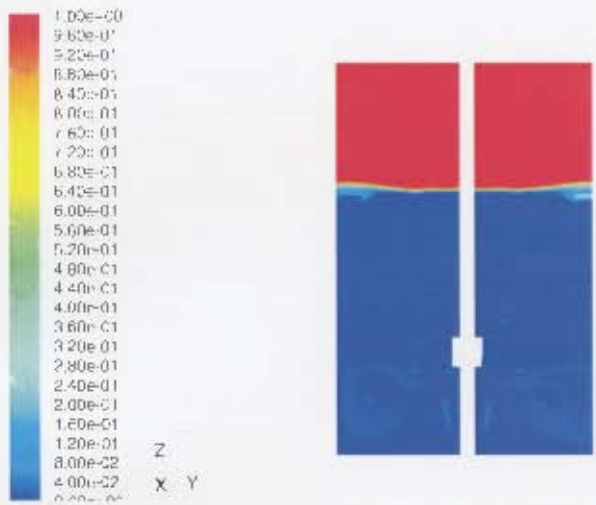

Figure 4.38: Contour plot at 630 rpm after 20 impeller rotations

Figure 4.39: Contour plot at 1260 rpm after 20 impeller rotations

Figure 4.40: Contour plot at 630 rpm after 30 impeller rotations

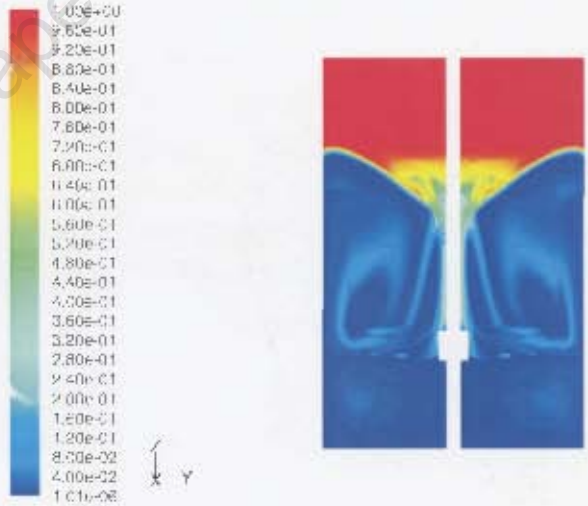

Figure 4.41: Contour plot at 1260 rpm after 30 impeller rotations

Discussion: Effect of Impeller Speed

The effect of the impeller speed on the gas-liquid interface was investigated. This was performed to support the fact that the discrepancy is rather due to the inability of the model to simulate such flows than a physically possible phenomenon. In addition to this, the model was validated in terms of the mean velocity, turbulence parameters, power number and gas hold-up. This was carried out at three different impeller speeds.

The mean velocities and turbulence parameters for the numerical and experimental work showed good

qualitative correlation with increasing values upon an increase in impeller speed. The parameters showed increases with increasing impeller speed. The mean velocities were under-predicted in the bulk region and over-predicted in the impeller stream and at impeller tip. The discrepancy was more considerable at higher impeller speed. Similar, observations were made by Engelbrecht (2006) for a single phase investigation. The root mean square velocity showed similar trends, but with better predictions at the impeller tip. The turbulent energy dissipation rates were under-predicted in the bulk region as observed for the other cases. An over-prediction was observed in the impeller stream and at the impeller tip. However, the over-prediction of the ε values was higher at the impeller tip. This shows that the standard $k-\varepsilon$ turbulence model used with the mixture model over-predicts the turbulence parameters. Hence, higher order discretisation schemes and finer grid resolution might be needed in this region (Wechsler et al., 1999; Deglon and Meyer, 2006). This also suggests a shortcoming of the mixture model with regards to the modelling of highly turbulent flows. The discrepancy observed in the other regions can be attributed to the experimental techniques used as outlined in Section 4.1.6.

The power draw prediction was acceptable. However, a small over-prediction was observed with increasing impeller speed. The disagreement to experimental data was more substantial at 1260 rpm. The relatively small amount of gas in the tank after the 30 impeller rotations modelled could have resulted on the higher power draw prediction. A higher amount of gas in the tank would have resulted in a lower mean fluid velocity at the impeller tip and hence a lower and better power draw values would have been predicted.

The gas hold-up was qualitatively well predicted in all cases with the common gas dispersion patterns. However, the gas-liquid interface was inaccurately modelled. The discrepancy was evident at 1260 rpm where the flow was completely unrealistic and unacceptable. It also caused a significant amount of gas entrainment into the tank, which resulted in a misleading and an inappropriate prediction of the gas hold-up. However, the phenomenon was less substantial at 630 rpm, where an insignificant amount of gas was entrained in the system. Thus, the modelling of the gas phase can be investigated at 630 rpm with the current modelling approach.

4.2.3 EFFECT OF DRAG MODEL

The standard Schiller drag model was based on a stagnant liquid without taking the effect of frothers into account. The effect of the frothers in the modelling of gas dispersion was found important by Engelbrecht (2006). The Schiller model was therefore modified to account for the effect of frothers by increasing the drag coefficient. This is explained in Section 4.2.3. Three cases were looked at, namely the case using the standard drag model (C1), and two other cases, C2 and C3, where the drag was increased by 41% and 71% respectively. The mixture model was used with a 360° geometry and the sliding mesh model was the impeller rotation model. The simulations were ran at 630 rpm where the inaccuracies with the modelling of the gas-liquid were minimal. The model was validated in terms of the mean velocities, turbulence parameters, power draw and gas hold-up, according the the experimental work presented by Deglon (1998). The results for the first 30 impeller rotations were described in the following sections.

Fluid Properties

The changes in the mean velocity values were insignificant with the increase in drag. In the bulk region and the impeller stream the increase in gas caused an insignificant decrease in velocity. The results at the impeller tip showed negligible or no difference in the mean velocity values over the 10 impeller rotation intervals.

Similar observations were obtained for the root mean square velocity values in the three different regions. The values were found unchanged with the increase in drag after the first 30 impeller rotations.

The turbulent energy dissipation rate at the impeller tip was unchanged in the bulk region and impeller stream over the 30 impeller rotations simulated. The increase in drag resulted in a decrease in the turbulent energy dissipation rate at the impeller tip.

Power Draw

The changes in power draw with the changes in the drag are shown in Figure 4.42. An insignificant increase in the power draw can be observed with an increase in drag. This is found to be contradictory with experimental data, since an increase in drag should have resulted in a decrease in the power draw.

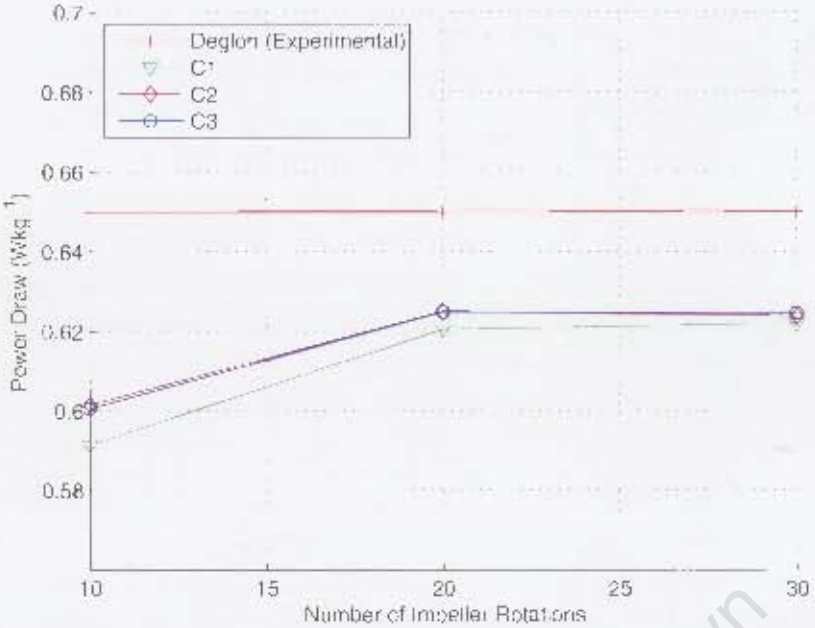

Figure 4.42: Power draw ($W.kg^{-1}$) vs impeller rotation

Gas Hold-Up

The gas hold-up for the three different drag coefficients over 30 impeller rotations is shown in Figure 4.43. The results under predicted the experimental data. However, good correlation with the experimental data was observed for the three cases, with a steady increase in the gas hold-up over time. The increase in drag coefficient led to an increase in the gas hold-up. However, negligible or no difference was obtained between C2 and C3. This is unclear since the two cases differ by a 40% increase in drag. This could mean that the increase in drag coefficient would not result in a proportional increase in gas hold-up.

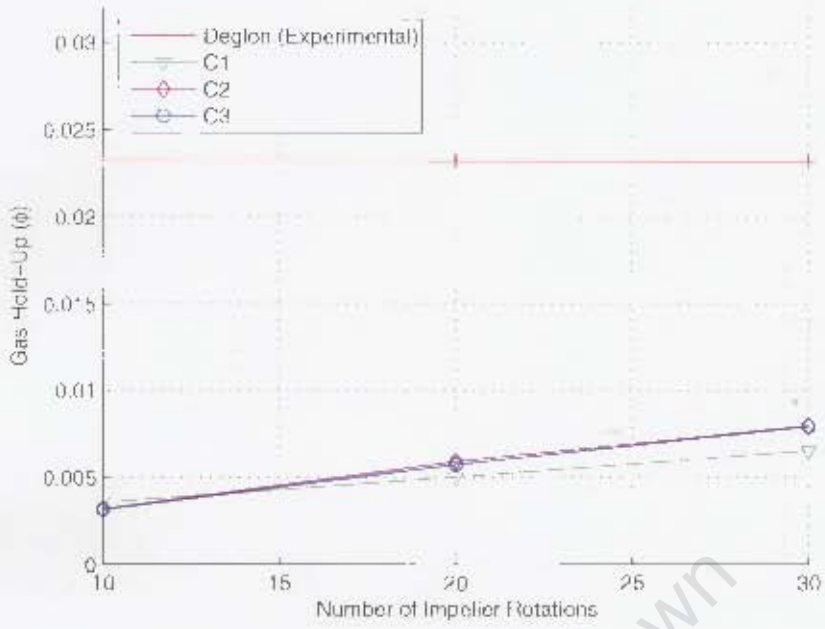

Figure 4.43: Gas hold-up (ϕ) vs impeller rotation

Discussion: Drag Model

The investigation of the effect of drag showed acceptable results in terms of the velocity values. The velocity was found to be unaffected or showed very small deviations which is most probably due to the different amount of gas in the system. However, at the impeller stream a decrease in the velocity was observed and was more evident, most probably due to the higher percentage of gas for the system with the system with the higher drag. Similar observations were made, where an increase in gas in the system resulted to a decrease in the root mean square velocity values. These observations were in good correlation with findings presented by Deglon (1998), where the author claimed that aeration led to a decrease in the mean fluid velocity. The turbulent energy values in the bulk region showed negligible change. This is most probably due the the fact that the bulk region was basically comprised of water and the effect of the drag model was minimal in that region. However, a decrease in the energy dissipation rate values was observed in the impeller stream and at the impeller tip. This was in contradiction to the findings made by Deglon (1998), who reported that aeration led to an increase in energy dissipation in those two regions.

The power draw was reasonably well predicted for all cases. However, the effect of the drag on the power draw was contradictory, since the higher volume of gas with a higher drag coefficient should have resulted in a decrease in the power draw. The increase in power can be attributed to the decrease in the turbulent energy dissipation rates obtained with the increase in drag.

The gas hold-up values increased with an increase in drag coefficient. However, the increase in drag did not result in a proportional increase in gas hold-up. The values for the 41% and 71% case were very similar.

5 CONCLUSIONS

The purpose of this investigation was to develop a multiphase model able to simulate the basic gas dispersion and the inherent hydrodynamics within the Rushton turbine agitated tank. This model was to be suitable to be used as the stepping stone for the modelling and investigation of gas-liquid related systems. The multiphase model was based on the previous numerical work of Siwale (2004) and on the recent work of Engelbrecht (2006). The models were compared and validated with the experimental work presented by Deglon (1998). The results were validated in terms of the mean velocities, the turbulence parameters, the power draw and the gas hold-up. Based on the results, the following conclusions were drawn.

5.1 STEADY STATE MODEL

The steady state model was found to be convenient for modelling the hydrodynamic phenomena. The mean velocity values were in good agreement with the experimental data, although they were under-predicted in the bulk region. This was attributed to the experimental accuracy due to the method used in determining fluid velocities. The poor prediction of the root mean square velocity determined from the turbulent kinetic energy was ascribed to the sampling technique used. Similarly, the discrepancy in the prediction of the turbulent energy dissipation rate was regarded as an experimental inaccuracy. The power draw showed good correlation for all cases. The value of the gas hold-up was poorly predicted, which was most probably due to the numerical instability upon introduction of air in the system.

The boundary conditions employed for the outlet was found to have negligible effect on the system. The convergence criterion were not met when a pressure outlet and outflow boundary was used. The system with a velocity outlet resulted in the accumulation of gas in the system. Thus, the steady state models were found inappropriate for the prediction of the gas phase. It is unclear whether it is due to the inherent unsteadiness of the system or just a numerical problem. However, the MRF model was found suitable for the prediction of the velocity values, the turbulence parameters and the power draw.

5.2 UNSTEADY STATE MODEL

The comparison of the mixture and Euler-Euler model over the first 30 impeller rotations showed that both models can be used for the prediction of the gas dispersion, velocities and the associated turbulence parameters. When compared, the velocity values were found to show the same correlation in the different regions in the tank. The root mean square turbulent velocity in bulk region and in the impeller stream were found to follow the same trend. However, at the impeller tip, the mixture model showed a better correlation to experimental data than the Euler-Euler model. The same observations were made for the prediction of the turbulent energy dissipation rate. This was attributed to the different turbulence models used, where the $k-\varepsilon$ dispersed model and the standard $k-\varepsilon$ turbulence model were used for the Euler-Euler model and the mixture model respectively. The considerable difference was mainly due to the high degree of turbulence in the region close to the impeller. The gas hold-up for the two models

showed the correlation over the 30 impeller rotations simulated. Thus, both multiphase models can be used for the prediction of the hydrodynamics in a gas-liquid system and for the modelling of gas dispersion.

The numerical results for the range of impeller speed showed good correlation to the experimental data. The disagreement to the experimental data observed, was attributed the experimental sampling techniques. However, the discrepancies were found more substantial with increasing impeller speed. The prediction of the turbulent energy dissipation rates was found to be over-predicted in all cases. Thus, the prediction of the turbulence parameters in regions of high turbulence with the standard $k - \varepsilon$ model in a multiphase system might not be adequate. This might be regarded as one of the shortcomings of the mixture model, where the system treating the phases on a volume fraction (mixture) basis fails to predict highly turbulent flows. The volume fraction of air was qualitatively well predicted, with the common gas distribution patterns. However, the models failed to accurately simulate the gas-liquid interface, resulting in the water rising to an unrealistic amount over the baffles. This was found to be exacerbated with increasing impeller speed. The multiphase model was found be inappropriate to model gas dispersion with the current modelling approach, and it was concluded that this could result in misleading and inaccurate predictions.

The approach used to account for frothers, by increasing the drag coefficient via the Schiller and Naumann correlation resulted in some unclear results. The mean and root mean square velocities decreased insignificantly with the increase in the volume fraction of gas in the tank. The turbulent energy dissipation rates decreased with increasing gas hold-up, disagreeing with the findings made by Deglon (1998). This supports the claim made with regards to the prediction of the turbulent energy dissipation rate while using the mixture model. The gas hold-up did not increase significantly with the increase in drag. This was unclear as a substantial increase in gas hold-up should have been obtained.

6 RECOMMENDATIONS

Recommendations made were based on the conclusions and are as followed:

The MRF model with the current modelling approach is unable to simulate gas-liquid systems due to its inability to simulate a numerically converged result. However, the model was adequate for the prediction of the velocity values, turbulence parameters and power draw. The model produced comparable results to the more computationally intensive sliding mesh model. Therefore, MRF model is unsuitable for the prediction of gas dispersion in stirred tanks.

The results between the mixture model and Euler-Euler model were comparable. Therefore, the mixture model can be used as an alternative multiphase model for the prediction of gas-dispersion, especially when computing power and time is limited.

Both models failed to correctly predict the fluid flow at the gas-liquid interface. The only acceptable solution was obtained at low impeller speeds. Thus, if the current modelling approach is used, it is recommended to be used only at low impeller speed.

The drag model gave acceptable results, with the increase in gas hold-up when the drag coefficient was increased. However, the modified model of Schiller and Naumann did not result in significant increase or decrease in values for the fluid properties, the power draw and most importantly the gas hold-up. Thus, further investigations are recommended.

REFERENCES

M.T Abujelala and D.G Lilley. Limitations and emperical extensions of the $k - \epsilon$ model as applied to turbulent confined swirling flows. *Chemical Engineering Communications*, 31:223–236, 1984.

P.M. Armenante, C. Luo, C. Chou, I. Fort, and J. Medek. Velocity profiles in a closed, unbaffled vessel: comparison between experimental and LDV data and numerical CFD predictions. *Chemical Engineering Science*, 52(20):3483–3492, 1997.

J. Aubin, D.F. Fletcher, and C. Xuereb. Modelling turbulent flow in stirred tanks with CFD: the influence of the modelling approach, turbulence model and numerical scheme. *Experimental Thermal And Fluid Science*, 28:431–445, 2004.

A. Bakker. *Hydrodynamics of stirred gas-liquid dispersions.* PhD thesis, Delft University of Technology, The Netherlands, 1992.

A. Bakker and H.E.A. Van Den Akker. A computational model for the gas-liquid flow in stirred reactors. *Institution of Chemical Engineers*, 72, Part A:594–606, 1994.

A. Brucato, M. Ciofalo, F. Grisafi, and G. Micale. Numerical prediction of flow fields in baffled stirred vessels: A comparison of alternative modelling approaches. *Chemical Engineering Science*, 53(21): 3653–3684, 1998.

J. Costes and J.P Coudrec. Study by laser doppler anemometry of the turbulent flow induced by a rushton turbine in a stirred tank:influence of the size of the units - i.mean flow and turbulence. *Chemical Engineering Science*, 43(10):2751–2764, 1988.

Louis A. Cutter. Flow and turbulence in a stirred tank. *American Institute Of Chemical Engineers Journal*, 1(12):35–45, 1966.

N.G. Deen, T. Solberg, and B.H. Hjertager. Flow generated by an aerated rushton impeller: Two-phase piv experiments and numerical simulations. *The Canadian Journal of Chemical Engineerinf*, 80:638–652, 2002.

D.A Deglon. *A hydrodynamic investigation of fine particle flotation in a batch flotation cell.* PhD thesis, University Of Cape Town, 1998.

D.A. Deglon and C.J Meyer. CFD modelling of stirred tanks: Numerical considerations. *Minerals Engineering*, 19:1059–1068, 2006.

J. Derksen and H.E.A. Van Den Akker. Large eddy simulations on the flow driven by rushton turbine. *American Institution of Chemical Engineers*, 45(2):209–221, 1999.

K.N. Dyster, E. Koutsakos, Z. Jaworski, and A.W. Nienow. An lda study of the radial discharge velocities generated by a rushton turbine: Newtonian fluids, re $\geq$ 5. *Institution of Chemical Engineers*, 71 Part A:11–23, 1993.

J.G.M. Eggels. Direct and large-eddy simulation of turbulent fluid flow using the lattice-boltzmann scheme. *International Journal of Heat and Fluid Flow*, 17:307–323, 1996.

D.F. Engelbrecht. Development of a CFD model for stirred tank applications. Master's thesis, University Of Cape Town, 2006.

D.F. Engelbrecht. CFD modeling of flow in a stirred tank. 2005.

Fluent Inc. *FLUENT® Users Guide.* Fluent Inc 2005.

M.D. Fokema, S.M. Kresta, and P.E. Wood. Importance of using the correct impeller boundary conditions for cfd simulations of stirred tanks. *Canadian Journal of Chemical Engineering*, 72:177–183, 1994.

R.I. Issa G. Tabor, A.D. Gosman. Numerical simulation of the flow in a mixing vessel stirred by a rushton turbine. *IChemE Symposium Series*, (140):25–34, 1996.

C. Gentric, D. Mignon, J. Bousquet, and P.A. Tanguy. Comparison of mixing in two gas-liquid reactors using CFD simulations. *Chemical Engineering Science*, 60:2253–2272, 2005.

A.D. Gosman, C. Lekakou, S. Politis, R.I. Issa, and M.K. Looney. Multidimensional modeling of turbulent two-phase flows in stirred vessels. *American Institution of Chemical Engineers*, 38(12):1946–1956, 1992.

H. Hartmann, J.J. Derksen, C. Montavon, J. Pearson, I.S. Hamill, and H.E.A. van den Akker. Assessment of large eddy and RANS stirred tank simulation by mean of LDA. *Chemical Engineering Science*, 59: 2419–2432, 2004.

A.D. Harvey-III, C.K. Lee, and S.E. Rogers. Steady-state modeling and experimental measurement of a baffled impeller stirred tank. *American Institute of Chemical Engineers*, 41(10):2177–2186, 1995.

K.H Javed, T. Mahmud, and J.M. Zhu. Numerical simulation of turbulent batch mixing in a vessel agitated by a rushton turbine. *Chemical Engineering and Processing*, 45:99–112, 2006.

Z. Jaworski and B. Zakrzewska. Modelling of the turbulent wall jet generated by a pitched blade turbine impeller: The effect of turbulence model. *Transactions of the Institution of Chemical Engineers*, 80 Part A:846–854, 2002.

M. Jenne and M. Reuss. A critical assessment on the use of the $k - \epsilon$ turbulence models for simulation of the turbulent liquid flow induced by a rushton-turbine in baffled stirred-tank reactors. *Chemical Engineering Science*, 54:3921–3941, 1991.

F. Kerdouss, A. Bannari, and P. Proulx. CFD modeling of gas dispersion and bubble size in a double turbine stirred tank. *Chemical Engineering Science*, 61:3313–3322, 2006.

A.R. Khopkar, A.R. Ramnohan, V.V. Ranade, and M.P. Dudukovic. Gas-liquid flow generated by a rushton turbine in stirred vessel:CARPT/CT measurements and CFD simulations. *Chemical Engineering Science*, 60:2215–2229, 2005.

S.M. Kresta and P.W. Wood. The flow field produced by a pitched blade turbine: Characterisation of the turbulence and estimation of the dissipation rate. *Chemical Engineering Science*, (10):1761–1774, 1993.

S.M. Kresta and P.W. Wood. Prediction of the three-dimensional turbulent flow in stirred tanks. *American Institute of Chemical Engineers*, 37(3):448–460, 1991.

G.L. Lane, M.P. Schwarz, and G.M Evans. Predicting gas-liquid flow in a mechanically stirred tank. *Applied Mathematical Modelling*, 26:223–235, 2002.

B.E. Launder and D.B Spalding. The numerical computation of turbulent flows. *Computer Methods in Applied Mechanics and Engineering*, 3(1974):269–289, 1974.

K.C. Lee and M. Yianneskis. The extent of periodicity of the flow in vessels stirred by rushton impellers. *In Industrial Mixing Technology: Chemical and Biological Applications, G.Tatterson (Ed.), American Institute of Chemical Engineers Series*, 90:5–18, 1994.

J.Y. Luo, A.D Gosman, R.I. Issa, J.C. Middleton, and M.K. Fitzgerald. Full flow field computation of mixing in baffled stirred vessels. *Transactions of the Institution of Chemical Engineers*, 71:342–344, 1993.

Elisabeth Marden and André Bakker. *Computational Fluid Mixing.* Fluent Inc, 2003.

P. Mavros. Flow visualisation in stirred vessels. a review of experimental techniques. *Transactions of the Institution of Chemical Engineers*, 79, Part A:113–127, 2001.

G. Montante, K.C. Lee, A. Brucato, and M. Yianneskis. Experiments and predictions of the transitions of the flow pattern with impeller clearance in stirred tanks. *Computers and Chemical Engineering*, 25: 729–735, 2001.

K.E. Morud and B.H. Hjertager. LDA measurements and CFD modeling of gas-liquid flow in stirred tanks. *Chemical Engineering Science*, 51(1996):233–249, 1996.

R. Newell. *Hydrodynamics and Scale-up in Rushton turbine flotation cells.* PhD thesis, University of South Australia, 2006.

K. Ng, N.J Fentiman, K.C. Lee, and M. Yianneskis. Assessment of sliding mesh CFD predictions and LDA measurements of the flow in a tank stirred by a rushton impeller. *Transactions of the Institution of Chemical Engineers*, 76:737–747, 1998.

B. Pyke. *Bubble-particle capture in turbulent flotation systems.* PhD thesis, Ian Wark Research Institute, University of South Australia, 2004.

Vivek V. Ranade. *Computational flow modeling for chemical reactor engineering.* Academic Press, 2002.

V.V. Ranade. An efficient computational model for simulating flow in stirred vessels: a case of rushton turbine. *Chemical Engineering Science*, 52(24):4473–4484, 1997.

V.V. Ranade and H.E.A. Van Den Akker. A computational snapshot of gas-liquid flow in baffled stirred reactors. *Chemical Engineering Science*, 49(24B):5175–5192, 1994.

V.V. Ranade and V.R Deshpande. Gas-liquid flow in stirred reactors: Trailing vortices and gas accumulation behind impeller blades. *Chemical Engineering Science*, 54:2305–2315, 1999.

V.V. Ranade, J.B. Joshi, and A.G. Marathe. Flow generated by pitched blade turbines II: Simulation using the $k - \varepsilon$ model. *Chemical Engineering Communications*, 81:225–248, 1989.

V.V. Ranade, M. Perrard, N. Le Sauze, C. Xuereb, and J. Bertrand. Trailing vortices of rushton turbine: PIV measurement and CFD simulations with snapshot approach. *Institution of Chemical Engineers*, 79 Part A, 2001.

K. Van Riet and John M. Smith. The trailing vortex system produced by rushton turbine agitators. *Chemical Engineering Science*, 30:1093–1105, 1975.

K. Van Riet and John M. Smith. The behaviour of gas-liquid mixtures near rushton turbine blades. *Chemical Engineering Science*, 28:1031–1037, 1973.

A.K. Sahu, P. Kumar, A.W. Patwardhan, and J.B. Joshi. CFD modelling and mixing in stirred tanks. *Chemical Engineering Science*, 54:2285–2293, 1999.

M. Shäfer, M. Höfken, and F.Durst. Detailed ldv measurement for visualisation of the flow field with a stirred-tank reactor equipped with a rushton turbine. *Institution of Chemical Engineers*, 75 Part A: 729–736, 1997.

N. Siwale. Modelling of flow in impeller stirred tanks using computational fluid dynamics. Master's thesis, University Of Cape Town, 2004.

P. Spicka, M.M. Dias, and J.C.B. Lopes. Gas-liquid flow in 2d column: Comparison between experimental data and CFD modelling. *Chemical Engineering Science*, 56:6367–6383, 2001.

H. Sun, Z. Mao, and G. Yu. Experimental and numerical study of gas hold-up in surface aerated stirred tanks. *Chemical Engineering Science*, 61:4098–4110, 2006.

G.B. Tatterson. *Fluid mixing and gas dispersion in agitated tanks.* McGraw Hill, Inc., 1991.

H.K Versteeg and W Malalasekera. *An Introduction to Computational Fluid Dynamics.* Pearson Prentice Hall, 1995.

K. Wechsler, M. Breuer, and F. Durst. Steady and unsteady computations of turbulent flows induced by a 4/45° pitched-blade impeller. *Journal of Fluid Engineering*, 121:318–329, 1999.

H. Wu and G.K. Patterson. Laser-doppler measurements of turbulent-flow parameters in a stirred mixer. *Chemical Engineering Science*, 44(10):2207–2221, 1989.

H. Wu, G.K. Patterson, and M. Van Doorn. Distribution of turbulence energy dissipation rates in a rushton turbine stirred mixer. *Experiments in Fluids*, 8:153–160, 1989.

Y. Zhang, A. Sam, and J.A Finch. Temperature effect on single bubble velocity profile in water and surfactant solution. *Colloids and Surfaces A*, 223:45–54, 2003.

Z.A. Zhou, N.O. Egiebor, and L.R. Plitt. Frother effects on bubble motion in a swarm. *Canadian Institute of Mining and Metallurgy*, 32(2):89–96, 1993.

A Steady State and Unsteady State Results Data

A.1 Steady State Results Data

A.1.1 Gas Hold-Up

Table A.1: Gas hold-up, ϕ

Iteration	Boundary		
	Outflow	Pressure Outlet	Velocity Inlet
5 000	0.0201	0.0197	0.0144
10 000	0.0321	0.0514	0.0249
15 000	0.0471	0.0677	0.0363
20 000	0.0501	0.0736	0.0456
25 000	0.0573	0.0769	0.0527
30 000	0.0647	0.080	0.0603

A.2 Unsteady State Results Data

A.2.1 Mean Velocity Data

Table A.2: Mean velocity, U ($m.s^{-1}$)

Impeller Speed (rpm)	Region								
	Bulk			Impeller Stream			Impeller Tip		
	Impeller Rotation								
	10	20	30	10	20	30	10	20	30
940 (Eulerian)	0.018	0.020	0.033	0.439	0.427	0.425	1.772	1.806	1.805
940 (Mixture)	0.025	0.030	0.051	0.425	0.401	0.392	1.768	1.799	1.793
630 (Mixture-C1)	0.019	0.025	0.033	0.246	0.248	0.247	1.160	1.186	1.191
630 (Mixture-C2)	0.018	0.027	0.029	0.220	0.210	0.228	1.150	1.184	1.192
630 (Mixture-C3)	0.016	0.027	0.030	0.230	0.208	0.224	1.150	1.184	1.192
1260 (Mixture)	0.074	0.068	0.094	0.570	0.541	0.520	2.404	2.424	2.403

A.2.2 Root Mean Sqaure Velocity Data

Table A.3: Root mean square velocity, $V_{R.M.S}$ $(m.s^{-1})$

Impeller Speed (rpm)	Region								
	Bulk			Impeller Stream			Impeller Tip		
	Impeller Rotation								
	10	20	30	10	20	30	10	20	30
940 (Eulerian)	0.138	0.113	0.115	0.380	0.379	0.378	0.422	0.340	0.396
940 (Mixture)	0.139	0.116	0.114	0.377	0.366	0.361	0.566	0.569	0.571
630 (Mixture-C1)	0.107	0.073	0.071	0.251	0.244	0.247	0.395	0.389	0.389
630 (Mixture-C2)	0.104	0.072	0.072	0.220	0.211	0.223	0.367	0.363	0.359
630 (Mixture-C3)	0.105	0.0730	0.072	0.230	0.208	0.224	0.366	0.362	0.359
1260 (Mixture)	0.183	0.163	0.159	0.514	0.499	0.492	0.802	0.804	0.800

A.2.3 Turbulent Energy Dissipation Rate Data

Table A.4: Turbulent energy dissipation rate, ϵ $(W.kg^{-1})$

Impeller Speed (rpm)	Region								
	Bulk			Impeller Stream			Impeller Tip		
	Impeller Rotation								
	10	20	30	10	20	30	10	20	30
940 (Eulerian)	0.150	0.132	0.149	11.82	12.73	12.86	28.0	25.95	25.57
940 (Mixture)	0.150	0.146	0.151	11.69	11.75	11.60	76.71	82.57	84.01
630 (Mixture-C1)	0.073	0.033	0.035	3.07	3.19	0.32	21.81	22.62	22.97
630 (Mixture-C2)	0.053	0.033	0.035	3.16	3.20	3.22	19.54	20.54	20.23
630 (Mixture-C3)	0.055	0.033	0.035	3.12	3.23	3.23	19.34	20.46	20.27
1260 (Mixture)	0.360	0.390	0.383	30.20	29.90	29.34	227.71	244.25	241.07

A.2.4 POWER DRAW DATA

Table A.5: Power draw, $(W.kg^{-1})$

Impeller Speed (rpm)	Impeller Rotation		
	10	20	30
940 (Eulerian)	2.01	2.19	2.19
940 (Mixture)	2.04	2.19	2.17
630 (Mixture-C1)	0.591	0.620	0.622
630 (Mixture-C2)	0.601	0.625	0.624
630 (Mixture-C3)	0.600	0.625	0.625
1260 (Mixture)	5.10	5.36	5.23

A.2.5 GAS HOLD-UP

Table A.6: Gas hold-up, (ϕ)

Impeller Speed (rpm)	Impeller Rotation		
	10	20	30
940 (Eulerian)	0.0261	0.0302	0.0328
940 (Mixture)	0.0086	0.0169	0.0259
630 (Mixture-C1)	0.0035	0.0050	0.0066
630 (Mixture-C2)	0.0031	0.0059	0.0080
630 (Mixture-C3)	0.0031	0.0057	0.0079
1260 (Mixture)	0.0171	0.0290	0.043